# A signal from inside the peroxisome initiates its division by promoting the remodeling of the peroxisomal membrane

Tong Guo, Christopher Gregg, Tatiana Boukh-Viner, Pavlo Kyryakov, Alexander Goldberg, Simon Bourque, Farhana Banu, Sandra Haile, Svetlana Milijevic, Karen Hung Yeung San, Jonathan Solomon, Vivianne Wong, and Vladimir I. Titorenko

Department of Biology, Concordia University, Montreal, Quebec H4B 1R6, Canada

We define the dynamics of spatial and temporal reorganization of the team of proteins and lipids serving peroxisome division. The peroxisome becomes competent for division only after it acquires the complete set of matrix proteins involved in lipid metabolism. Overloading the peroxisome with matrix proteins promotes the relocation of acyl-CoA oxidase (Aox), an enzyme of fatty acid β-oxidation, from the matrix to the membrane. The binding of Aox to Pex16p, a membrane-associated peroxin required for peroxisome biogenesis, initiates the biosynthesis of phosphatidic acid and diacylglycerol (DAG) in the membrane. The formation of these two lipids and the subsequent transbilayer movement of DAG initiate the assembly of a complex between the peroxins Pex10p and Pex19p, the dynamin-like GTPase Vps1p, and several actin cytoskeletal proteins on the peroxisomal surface. This protein team promotes membrane fission, thereby executing the terminal step of peroxisome division.

## Introduction

To be accurately partitioned during cell division and inherited by the daughter cells, organelles must double in size and divide during the cell cycle (Shorter and Warren, 2002; Osteryoung and Nunnari, 2003; Yan et al., 2005). The division of mitochondria and chloroplasts, the two endosymbiotic organelles that are surrounded by inner and outer membranes, is uncoupled from cell division and requires the FtsZ-like and/or dynamin-related GTPases (Osteryoung and Nunnari, 2003). In contrast, the division of the Golgi apparatus, an organelle of the secretory pathway that is bound by a single membrane, is coupled to the cell division cycle and is served by a division machinery that is unique for this nonendosymbiotic organelle (Shorter and Warren, 2002; Colanzi et al., 2003). Similar to Golgi and in contrast to endosymbiotic organelles, peroxisomes derive from the endoplasmic reticulum (Titorenko and Mullen, 2006) and are surrounded by a single membrane. On the other hand, akin to mitochondria and chloroplasts and contrary to Golgi, peroxisomes require dynamin-related GTPases for their division that is uncoupled from cell division (Thoms and Erdmann, 2005; Yan et al., 2005). Moreover, the peroxisomal and mitochondrial division machineries in mammalian cells share at least two essential protein components (Schrader, 2006). Although the mechanisms by which mitochondria, chloroplasts, and Golgi divide are well defined (Shorter and Warren, 2002; Osteryoung and Nunnari, 2003; Corda et al., 2006), the molecular mechanism for the integration of multiple components of the peroxisomal division machinery remains to be established (Thoms and Erdmann, 2005; Schrader, 2006).

We study peroxisome division in the yeast *Yarrowia lipolytica*. Similar to peroxisomes in humans and in other yeast species (Titorenko and Mullen, 2006), peroxisomes in *Y. lipolytica* do not grow and divide at the same time (Guo et al., 2003). The growth of immature peroxisomal vesicles, termed P1–P5, which is accomplished by the stepwise import of distinct subsets of matrix proteins, and their development into mature peroxisomes P6 occur before completely assembled mature peroxisomes undergo division. The division of mature peroxisomes in *Y. lipolytica* is regulated by an unusual mechanism that controls membrane fission in response to a signal emanating from within the peroxisome (Guo et al., 2003). The import of matrix proteins

T. Guo and C. Gregg contributed equally to this paper.

Correspondence to Vladimir I. Titorenko: vtitor@alcor.concordia.ca

Abbreviations used in this paper: Aox, acyl-CoA oxidase; DAG, diacylglycerol; LPA, lyso-PA; LPAAT, LPA acyltransferase; n-OG, n-octyl-β-D-glucopyranoside; PA, phosphatidic acid; PAP, PA phosphatase; PC, phosphatidylcholine; PE, phosphatidylethanolamine; PI, phosphatidylinositol; PMP, peroxisomal membrane protein; PS, phosphatidylserine.

The online version of this article contains supplemental material.


The Journal of Cell Biology, Vol. 177, No. 2, April 23, 2007 289–303
http://www.jcb.org/cgi/doi/10.1083/jcb.200609072

into different immature intermediates along the peroxisome assembly pathway provides them with an increasing fraction of the matrix proteins present in mature peroxisomes. The increase in the total mass of matrix proteins above a critical level causes the redistribution of a peroxisomal protein, acyl-CoA oxidase (Aox), from the matrix to the membrane. A substantial redistribution of Aox occurs only in mature peroxisomes, which contain the greatest percentage of matrix proteins. Inside mature peroxisomes, the membrane-bound pool of Aox interacts with Pex16p. Pex16p is a membrane-associated peroxin that negatively regulates the membrane fission event required for the division of immature peroxisomal vesicles, thereby preventing their excessive proliferation (Guo et al., 2003). The interaction between membrane-attached Aox and Pex16p terminates the negative action of Pex16p on fission of the peroxisomal membrane, thereby allowing mature peroxisomes to divide. Akin to other membrane fission events (Chernomordik and Kozlov, 2003; McMahon and Gallop, 2005; Zimmerberg and Kozlov, 2006), fission of the peroxisomal membrane must be preceded by the destabilization of the membrane bilayer and strong membrane bending. These energetically unfavorable processes require several teams of proteins and a distinct set of membrane lipids, including phosphoinositides, phosphatidic acid (PA), and diacylglycerol (DAG; Bankaitis, 2002; Farsad and De Camilli, 2003; Behnia and Munro, 2005; McMahon and Gallop, 2005; Corda et al., 2006).

Here, we investigate how the interaction between Pex16p and Aox promotes the division of mature peroxisomes. We demonstrate that the Pex16p- and Aox-dependent intraperoxisomal signaling cascade activates the biosynthesis and transbilayer movement of a distinct set of membrane lipids. The resulting remodeling of the lipid repertoire of the membrane bilayer initiates the stepwise assembly of a multicomponent protein complex on the surface of the mature peroxisome. This newly assembled protein complex carries out membrane fission, thereby executing the terminal step of peroxisome division.

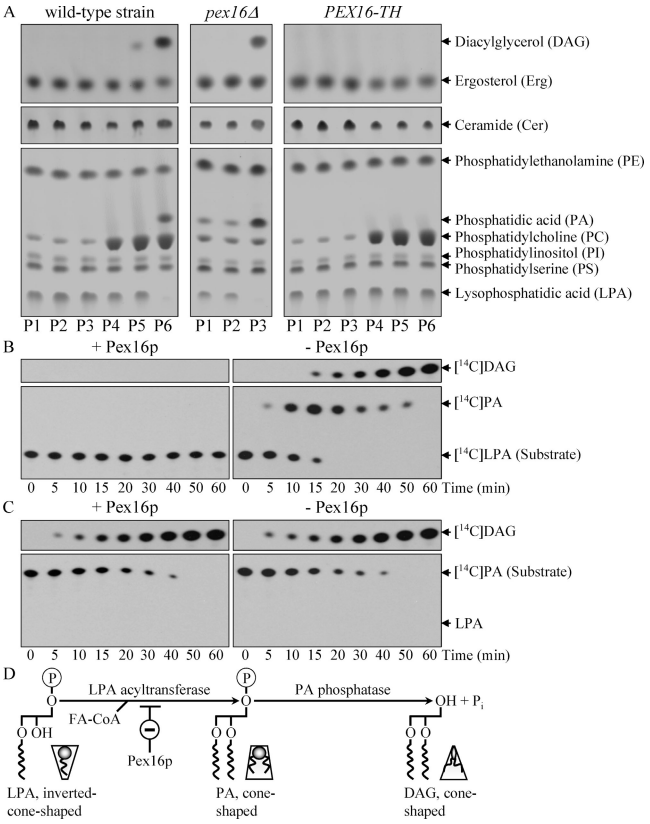


Figure 1. **Pex16p regulates lipid metabolism in the peroxisomal membrane.** (A) Spectra of membrane lipids in different peroxisomal subforms purified from wild-type, *pex16Δ*, and *PEX16-TH* cells. Peroxisomes were osmotically lysed and subjected to centrifugation. Lipids were extracted from equal quantities of the pelleted membrane proteins and analyzed by TLC. (B and C) Dynamics of radiolabeled lipids in the membrane of P1 liposomes. Liposomes were reconstituted from PMPs immunodepleted (−Pex16p) or not immunodepleted (+Pex16p) of Pex16p and from nonradiolabeled lipids, all of which were extracted from the membrane of immature peroxisomal vesicles P1. [$^{14}$C]LPA (B) or [$^{14}$C]PA (C) were the only radiolabeled lipids incorporated into liposomes during their reconstitution. The [$^{14}$C]LPA-loaded liposomes (B) were also supplemented with unlabeled oleoyl-CoA, a cosubstrate of LPAAT. Samples were taken at the indicated times after transfer of reconstituted liposomes from ice to 26°C. Lipids were extracted from the membrane and analyzed by TLC. (D) Pex16p inhibits LPAAT, the first enzyme in a two-step biosynthetic pathway leading to the formation of DAG in the peroxisomal membrane during conversion of P5 to P6.

## Results

### Lipid composition of the peroxisomal membrane is changed during the last step of the assembly of the division-competent mature peroxisome

In wild-type cells, the levels of PA and DAG in the peroxisomal membrane dramatically increased only during conversion of immature peroxisomal vesicles P5 to mature peroxisomes P6 (Fig. 1 A). These two cone-shaped lipids are potent inducers of membrane bending and fission (Kooijman et al., 2003; Shemesh et al., 2003). In contrast, the level of lyso-PA (LPA), an inverted cone–shaped lipid (Kooijman et al., 2003), in the membrane greatly reduced during conversion of P5 to P6 (Fig. 1 A). Importantly, the lack of Pex16p in *pex16Δ* mutant cells resulted in the accumulation of PA and DAG and led to the disappearance of LPA even in the membrane of immature peroxisomal vesicles P3 (Fig. 1 A). The *pex16Δ* mutation, which causes the excessive proliferation of immature peroxisomal vesicles (Guo et al., 2003), impaired the conversion of P3 to P4 (unpublished data). On the contrary, the *PEX16-TH* mutation, which averts peroxisome division by dramatically elevating the intraperoxisomal pool of Pex16p (Guo et al., 2003), abolished the formation of PA and DAG and prevented the disappearance of LPA even in the membrane of P6 (Fig. 1 A). These findings suggest that the interaction between Aox and Pex16p at the matrix face of the membrane of mature peroxisomes activates the biosynthesis of PA and DAG and promotes the catabolism of LPA.

To elucidate the mechanism that regulates the levels of PA, DAG, and LPA in the peroxisomal membrane, we reconstituted peroxisomal liposomes from detergent-solubilized peroxisomal membrane proteins (PMPs) and membrane lipids of immature peroxisomal vesicles P1. No Aox subunits are attached to the membrane inside these liposomes (Guo et al., 2003), in which Pex16p is present only in its free form. In the membrane

of P1 liposomes supplemented with [$^{14}$C]LPA as the only radiolabeled lipid, the decline in the level of [$^{14}$C]LPA coincided with the increase in the amount of newly synthesized [$^{14}$C]PA, which preceded the appearance of [$^{14}$C]DAG, only if these liposomes were reconstituted from PMPs immunodepleted of Pex16p (Fig. 1 B). In contrast, if [$^{14}$C]PA was used as the only radiolabeled membrane lipid for reconstituting P1 liposomes, the decline in its level coincided with the increase in the amount of newly synthesized [$^{14}$C]DAG even if the PMPs taken for liposome reconstitution were not immunodepleted of Pex16p (Fig. 1 C).

Altogether, our findings provide evidence that (1) the conversion of P5 to P6 is marked by the biosynthesis of PA and DAG in the peroxisomal membrane; (2) PA and DAG are formed in a two-step biosynthetic pathway, which includes two consecutive enzymatic reactions catalyzed by an LPA acyltransferase (LPAAT) and a PA phosphatase (PAP; Fig. 1 D); and (3) Pex16p, a negative regulator of the division of immature peroxisomal vesicles (Guo et al., 2003), inhibits LPAAT.

The LPAAT and PAP reactions are the only reactions leading to the formation of PA and DAG, respectively, in the peroxisomal membrane. In fact, this membrane lacked the activities of all other enzymes that can promote the biosynthesis of PA or DAG (Hannun et al., 2001; Bankaitis, 2002; De Matteis et al., 2002), including phospholipase D, inositol phosphosphingolipid phospholipase C (PLC), phosphoinositide-specific PLC, DAG kinase, inositol phosphorylceramide synthase, and inositolphosphotransferase 1 (Fig. S1, available at http://www.jcb.org/cgi/content/full/jcb.200609072/DC1).

We purified LPAAT and PAP from the membrane of P6 (Fig. 2 A). Purified LPAAT and PAP were identified by mass spectrometry as Slc1p, an acylglycerol-3-phosphate acyltransferase (Athenstaedt and Daum, 1999), and Dpp1p, a DAG pyrophosphate phosphatase (Carman and Han, 2006), respectively. Using highly purified peroxisomes of wild-type cells, we found that all six peroxisomal subforms have similar amounts of both Slc1p (LPAAT) and Dpp1p (PAP; Fig. 2 B). Akin to the peroxisomal integral membrane protein Pex2p (Titorenko et al., 1996) and in contrast to the peroxisomal peripheral membrane protein Pex16p (Eitzen et al., 1997), neither Slc1p (LPAAT) nor Dpp1p (PAP) was solubilized by either 1 M NaCl or 0.1 M $Na_2CO_3$ (pH 11.0; Fig. 2 C). Thus, both Slc1p (LPAAT) and Dpp1p (PAP) are integral membrane proteins. Furthermore, like Pex16p attached to the lumenal face (Eitzen et al., 1997) and unlike the peripheral membrane protein Pex19p on the cytosolic face of peroxisomes (Subramani et al., 2000; Lambkin and Rachubinski, 2001), both Slc1p (LPAAT) and Dpp1p (PAP) were resistant to digestion by external protease added to intact peroxisomes (Fig. 2 D). Altogether, these data imply that, in all six peroxisomal subforms, both Slc1p (LPAAT) and Dpp1p (PAP) are integral membrane proteins that do not face the cytosol, being integrated into the lumenal leaflet of the membrane.

Importantly, the lack of LPAAT in *slc1Δ* mutant cells abolished the formation of PA and DAG and prevented the disappearance of LPA in the membrane of P6 (Fig. 2 E) and resulted in a reduced number of greatly enlarged mature

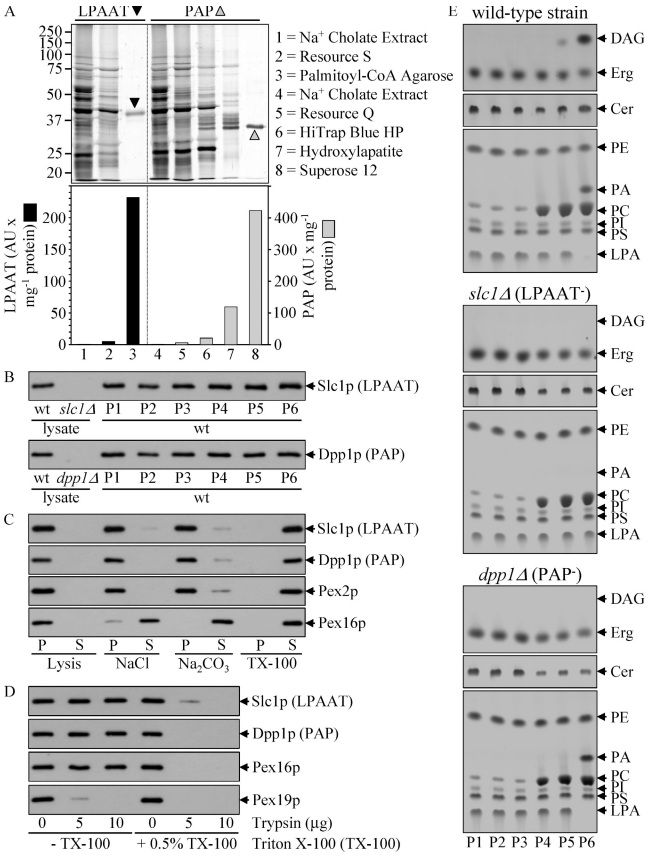


Figure 2. **In all six peroxisomal subforms, both LPAAT and PAP are integral membrane proteins that do not face the cytosol and are crucial for the biosynthesis of PA and DAG in the peroxisomal membrane.** (A) Purification of LPAAT and PAP from the membrane of mature peroxisomes P6. Peroxisomes of wild-type strain were osmotically lysed and subjected to centrifugation. Pelleted membrane proteins were extracted with $Na^+$ cholate and subjected to a series of the chromatographic purification steps, as indicated. Proteins recovered in the $Na^+$ cholate-extracted membrane of P6 and in chromatographic fractions were resolved by SDS-PAGE, followed by silver staining. For monitoring enzymatic activities of LPAAT and PAP, recovered membrane proteins were incorporated into the membrane of peroxisomal liposomes that were reconstituted from the PMPs and membrane lipids of P6. [$^{14}$C]-labeled lipid substrates of LPAAT and PAP were incorporated into liposomes as described in the legend to Fig. 1. The spectra of proteins and enzymatic activities of LPAAT and PAP recovered in the $Na^+$ cholate–extracted membrane of P6 and in the peak chromatographic fractions are shown. Arrowheads mark LPAAT and PAP, which were purified to apparent homogeneity and identified by mass spectrometry as the Slc1p and Dpp1p proteins, respectively. (B) Peroxisomal subforms P1–P6 were purified from wild-type (wt) cells. Equal quantities (10 μg) of protein from these peroxisomes, as well as equal quantities (100 μg) of protein from lysates of whole cells of wild-type, *slc1Δ*, and *dpp1Δ* strains, were analyzed by immunoblotting with antibodies to Slc1p (LPAAT) and Dpp1p (PAP). (C) Equal aliquots (10 μg of total protein) of mature peroxisomes purified from wild-type cells were osmotically lysed or exposed to 1 M NaCl, 0.1 M $Na_2CO_3$, pH 11.0, or 0.5% (vol/vol) Triton X-100. After incubation on ice for 30 min, samples were separated into supernatant (S) and pellet (P) fractions by centrifugation and then immunoblotted with the indicated antibodies. (D) Equal aliquots (10 μg of total protein) of mature peroxisomes purified from wild-type cells were treated with the indicated amounts of trypsin in the absence (−) or presence (+) of 0.5% (vol/vol) Triton X-100 for 30 min on ice. Samples were subjected to SDS-PAGE and immunoblotting with the indicated antibodies. (E) Spectra of membrane lipids in different peroxisomal subforms purified from wild-type, *slc1Δ*, and *dpp1Δ* cells. Peroxisomes were osmotically lysed and subjected to centrifugation. Lipids were extracted from equal quantities of the pelleted membrane proteins and analyzed by TLC.

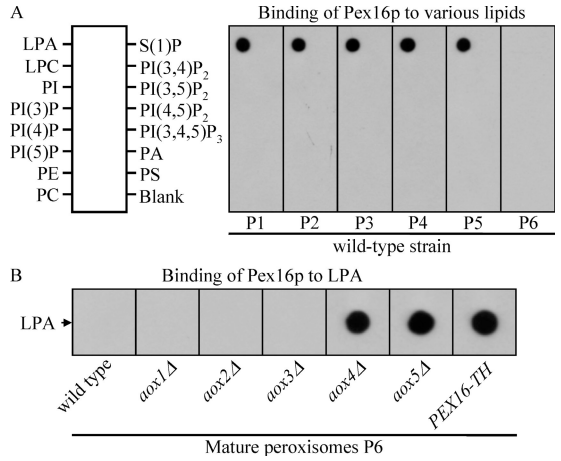


Figure 3. **Pex16p binds to LPA only in the membranes of division-incompetent peroxisomal subforms.** Different peroxisomal subforms purified from wild-type cells (A) and highly purified mature peroxisomes P6 of wild-type and mutant strains (B) were osmotically lysed and subjected to centrifugation. The pellet of membranes after such centrifugation was solubilized with a detergent, n-OG. Equal quantities of detergent-soluble membrane proteins were analyzed by protein-lipid overlay assay using commercial PIP Strips. Pex16p was detected by immunoblotting with anti-Pex16p antibodies.

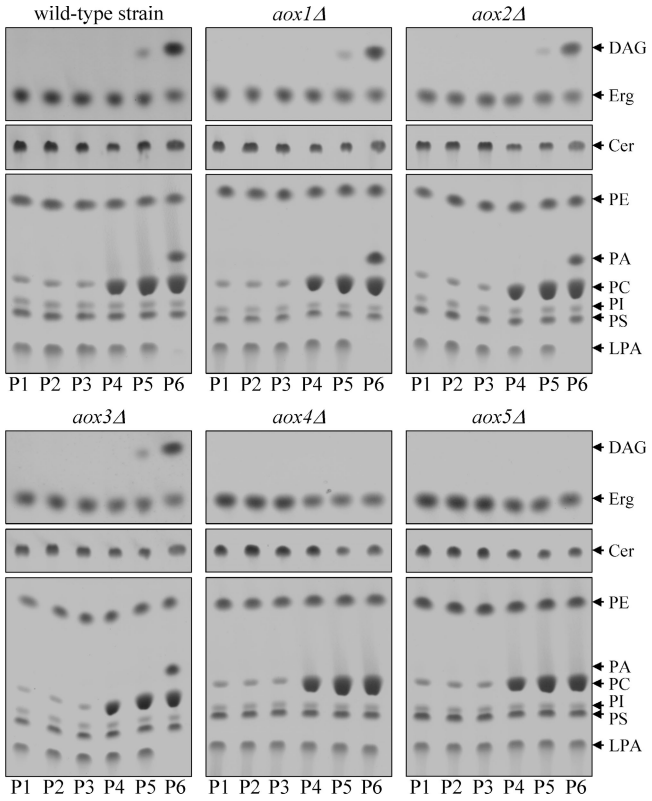


Figure 4. **Mutations that abolish the binding of Aox to Pex16p, thereby impairing peroxisome division, prevent the biosynthesis of PA and DAG in the peroxisomal membrane.** Highly purified peroxisomal subforms were osmotically lysed and subjected to centrifugation. Equal quantities of the pelleted membrane proteins recovered from different peroxisomal subforms were subjected to lipid extraction, which was followed by TLC and visualization of lipids.

peroxisomes (Fig. S2, A, B, G, and H, available at http://www.jcb.org/cgi/content/full/jcb.200609072/DC1). Moreover, the lack of PAP in *dpp1Δ* mutant cells (1) did not impair the Slc1p (LPAAT)-dependent biosynthesis of PA from LPA in the membrane of P6 (Fig. 2 E); (2) prevented the conversion of PA to DAG in the membrane of P6 (Fig. 2 E); and (3) resulted in fewer, but greatly enlarged, mature peroxisomes (Fig. S2, A, C, G, and H). Altogether, our findings provide evidence that (1) both the Slc1p (LPAAT)-dependent formation of PA from LPA and the subsequent Dpp1p (PAP)-dependent biosynthesis of DAG from PA, which occur in the lumenal leaflet of the peroxisomal membrane only during conversion of P5 to P6, are essential for the division of P6, and (2) although the biosynthesis of PA is necessary for the division of P6, the presence of PA alone is not sufficient for promoting this process, which also requires the biosynthesis of DAG. It remains to be established whether DAG alone stimulates peroxisome division or, alternatively, the simultaneous presence of PA and DAG in the membrane of P6 is mandatory for its fission.

### The binding of Pex16p to LPA prevents the formation of PA and DAG in the membranes of immature peroxisomal vesicles

Because Pex16p inhibits LPAAT in the membranes of P1–P5, thereby preventing the formation of both PA and DAG, we sought to define the mechanism for the negative regulation of LPAAT by Pex16p in immature peroxisomal vesicles. Pex16p solubilized with the detergent n-octyl-β-D-glucopyranoside (n-OG) from the membranes of P1–P5 purified from wild-type cells was able to bind only to LPA, a substrate of LPAAT, but not to any other lipid tested (Fig. 3 A). In contrast, n-OG–soluble Pex16p of mature peroxisomes P6 did not bind to LPA if these peroxisomes were recovered from wild-type or *aox1Δ*, *aox2Δ*, and *aox3Δ* mutant strains (Fig. 3). All these strains lack LPA and carry both PA and DAG in the membranes of their division-competent mature peroxisomes (Fig. 1 A and Fig. 4). Of note, Pex16p is attached to the membranes of immature peroxisomal vesicles only in its free form, whereas all the Pex16p on the inner face of mature peroxisomes of wild-type or *aox1Δ*, *aox2Δ*, and *aox3Δ* mutant cells is titrated by its interaction with Aox (Guo et al., 2003). Importantly, the interaction between Pex16p and Aox is not affected by n-OG. Altogether, these data suggest that the binding of Aox to Pex16p in mature peroxisomes of wild-type cells greatly decreases the affinity between Pex16p and LPA, thereby allowing LPA to enter the two-step biosynthetic pathway leading to the formation of PA and DAG. This hypothesis is supported by the observation that n-OG–soluble Pex16p of mature peroxisomes was capable of binding to LPA if these mature peroxisomes were purified from *aox4Δ*, *aox5Δ*, or *PEX16-TH* strains (Fig. 3 B). All these mutant strains carry Pex16p in a free form that is not titrated by its interaction with Aox, are deficient in the division of mature peroxisomes, and accumulate a reduced number of greatly enlarged mature peroxisomes (Guo et al., 2003) that contain LPA but lack both PA and DAG (Fig. 1 A and Fig. 4).

### Dynamics of changes in the transbilayer distribution of DAG and phosphatidylserine (PS) in the peroxisomal membrane during peroxisome maturation

Our data suggest that LPA enters the two-step pathway for the biosynthesis of PA and DAG (Fig. 1 D) only when the efficiency of its binding to Pex16p declines. Pex16p is a peripheral membrane protein that is attached only to the lumenal leaflet of the peroxisomal membrane (Eitzen et al., 1997). Furthermore, it seems unlikely that LPA can translocate from the lumenal to the cytosolic leaflet of the peroxisomal membrane, as its spontaneous transbilayer movement is very slow (Holthuis and Levine, 2005). Moreover, neither LPAAT nor PAP faces the cytosol, being integrated into the lumenal leaflet of the peroxisomal membrane (Fig. 2, C and D). Altogether, these findings imply that the biosynthesis of PA and DAG is spatially restricted to the lumenal leaflet of the peroxisomal membrane.

To evaluate the arrangement of DAG between the two leaflets of the membrane bilayers in different peroxisomal subforms, we reconstituted two types of resealed peroxisomes, termed RPA and RPB, from osmotically lysed intact peroxisomes. RPA were reconstituted in a MES-based buffer at pH 5.5, whereas RPB was made in a Hepes-based buffer at pH 7.5. Similar to intact peroxisomes (Titorenko et al., 2000), both RPA and RPB could float out of the most dense sucrose during centrifugation to equilibrium in sucrose density gradients (Fig. S3 A, available at http://www.jcb.org/cgi/content/full/jcb.200609072/DC1) and were bound by a single membrane (Fig. S3 C). In intact peroxisomes, Pex19p is a peripheral membrane protein that resides on the cytosolic face of the peroxisome, whereas the peripheral membrane protein Pex16p is attached to its lumenal face (Fig. S3, B and D). In RPA, most of Pex19p, but only a minor portion of Pex16p, was accessible to trypsin and to the corresponding antigen-specific IgG molecules exogenously added to this type of resealed peroxisomes (Fig. S3, B and D). Thus, the membrane delimiting most of the RPA species formed during peroxisome resealing was present in the outside-out orientation, whereas only a minor fraction of RPA species had their membrane resealed in the inside-out orientation. In contrast, in RPB, only a minor portion of Pex19p, but most of Pex16p, was accessible to trypsin and to the corresponding antigen-specific IgG molecules exogenously added to this type of resealed peroxisomes (Fig. S3, B and D). Hence, only a minor fraction of RPBs had their membrane resealed in the outside-out orientation, whereas the membrane delimiting most of the RPB species formed during peroxisome resealing was present in the inside-out orientation. Using a Pex19p-specific fluorescent probe, we calculated the percentages of outside-out– and inside-out–oriented species of RPA and RPB that were formed by resealing of osmotically lysed peroxisomal subforms P1–P6 (Fig. S3, E and F).

The ability to calculate the percentage of outside-out– and inside-out–oriented species of RPA and RPB allowed us to calculate the percentage of DAG residing in the cytosolic and lumenal leaflets of the membrane bilayers in intact peroxisomes. The DAG-binding C1b domain of protein kinase C (Johnson et al., 2000) labeled with the fluorophore Alexa Fluor 488 was used as a DAG-specific fluorescent probe. In intact P5, only $13 \pm 4\%$ of the total pool of DAG was detected in the cytosolic leaflet of the membrane bilayer (Fig. S3 H). Thus, DAG resides predominantly in the lumenal membrane leaflet of P5. In contrast, DAG is distributed symmetrically between the two leaflets of the membrane bilayer in mature peroxisomes P6. In fact, $57 \pm 3\%$ of this lipid resided in the cytosolic membrane leaflet of P6 (Fig. S3 H).

We then used monoclonal antibodies to PS, a lipid that has a cylindrical shape (Sprong et al., 2001), to monitor its transbilayer distribution in the membranes of different peroxisomal subforms. PS in the membranes of immature peroxisomal vesicles P1–P3 resides predominantly in their cytosolic leaflets (Fig. S3 H). As peroxisomes mature, PS gradually moves from the cytosolic to the lumenal leaflets of their membranes. Indeed, only $15 \pm 1\%$ of this lipid resided in the cytosolic membrane leaflet of P6 (Fig. S3 H). In summary, the assembly of mature peroxisomes promotes the specific redistribution of DAG and PS between the two leaflets of the peroxisomal membrane. The movement of DAG from the lumenal to the cytosolic leaflet of the membrane bilayer coincides with the translocation of PS in the opposite direction.

### ER-derived phosphatidylcholine (PC) in the peroxisomal membrane activates both LPAAT and PAP

The levels of PC, a major glycerophospholipid of the peroxisomal membrane (Schneiter et al., 1999), in P4, P5, and P6 peroxisomes of wild-type cells were substantially higher than in P1, P2, and P3 peroxisomes (Fig. 1 A). The observed increase in the levels of PC was not due to its de novo synthesis. In fact, the membranes of P3 and P4 did not contain PA and DAG (Fig. 1 A), two substrates for PC biosynthesis via the phosphatidylethanolamine (PE) methylation and cytidine diphosphate–choline pathways, respectively (Bankaitis, 2002). Thus, PC is transported to the membranes of P3 and P4 during their conversion to P4 and P5, respectively. Three established mechanisms of intracellular lipid transport to organellar membranes include transport catalyzed by cytosolic lipid transfer proteins (Munro, 2003; Holthuis and Levine, 2005), vesicle-mediated transport (Sillence and Platt, 2004; van Meer and Sprong, 2004), and transport at regions of close apposition between specialized microdomains of the ER membrane and the membranes of the trans-Golgi or mitochondria (Holthuis and Levine, 2005; Voelker, 2005). Our data imply that PC is transferred from the donor membrane of a distinct subcompartment of the ER to the acceptor membranes of P3 and P4 associated with this subcompartment and that this transfer of PC requires the peroxisome-associated peroxin Pex2p, provides membranes of P3 and P4 with the bulk quantities of PC, and is essential for the conversion of P4 to P5. This hypothesis is based on the following findings. First, a distinct form of the ER copurifies with P3 and P4 peroxisomes and can be separated from them by treatment with EDTA (Titorenko et al., 1996, 2000). Second, the P3- and P4-associated ER subcompartment can be distinguished from the free form of the ER by buoyant density and the total level of membrane glycerophospholipids (Titorenko et al., 1996), as

well as by protein spectrum (Fig. S4 B, available at http://www.jcb.org/cgi/content/full/jcb.200609072/DC1). Third, the *pex2Δ* mutation increases the levels of membrane glycerophospholipids in the P3- and P4-associated subcompartment of the ER (Titorenko et al., 1996), substantially decreases the level of PC in P4 (Fig. S4 A), and impairs its conversion to P5 (unpublished data).

It seems that PC in the peroxisomal membrane is a positive regulator of both LPAAT and PAP. In fact, the specific activities of these two membrane-bound enzymes in liposomes reconstituted from the Pex16p-immunodepleted PMPs and membrane lipids of P1, P2, and P3 were substantially lower than in liposomes reconstituted from membrane components of P4, P5, and P6 (Fig. 5, A and B). Of note, LPAAT and PAP activities detected in the membranes of these peroxisomal liposomes were proportional to the steady-state levels of PC recovered in these membranes (Fig. 5, A and B). Importantly, the positive effect of PC on both LPAAT and PAP could be reconstructed in four different types of the Pex16p-immunodepleted liposomes that were reconstituted from membrane components of P1, P2, or P3 and varied only in the quantities of PC present in their membranes (Fig. 5, C–F). Noteworthy, by rising the quantities of PC in the membranes of P1-, P2-, and P3-based liposomes to the levels comparable to those present in the membranes of P4-, P5-, and P6-based liposomes, both LPAAT and PAP could be substantially stimulated, matching their enzymatic activities in liposomes reconstituted from membrane components of P4, P5, and P6 (Fig. 5, E and F). Considering that all six peroxisomal subforms have similar amounts of both LPAAT and PAP (Fig. 2 B), the findings reported in Fig. 5 support the notion that PC in the peroxisomal membrane activates these two enzymes.

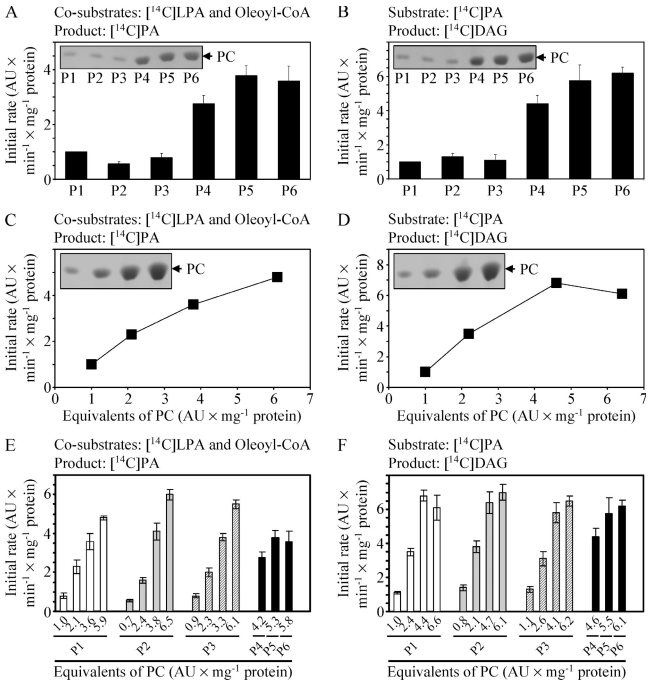


Figure 5. **PC in the peroxisomal membrane is a positive regulator of both LPAAT and PAP.** (A and B) The initial rates of the LPAAT (A) and PAP (B) reactions and the levels of PC recovered in the membranes of liposomes reconstituted from the Pex16p-immunodepleted PMPs and membrane lipids of different peroxisomal subforms. Peroxisomal liposomes that lack Pex16p were reconstituted as described in the legend to Fig. 1. [$^{14}$C]-labeled lipid substrates were incorporated into liposomes during their reconstitution. (C–F) The initial rates of the LPAAT (C and E) and PAP (D and F) reactions and the levels of PC recovered in the membranes of four different types of liposomes reconstituted from the Pex16p-immunodepleted PMPs and membrane lipids of P1 (C– F), P2 (E and F), or P3 (E and F) peroxisomes. These four different types of P1-, P2-, or P3-based liposomes varied only in the quantities of PC used for their reconstitution and recovered in their membranes after the reconstitution. For comparison, the initial rates of the LPAAT (E) and PAP (F) reactions and the levels of PC recovered in the membranes of liposomes reconstituted from the Pex16p-immunodepleted PMPs and membrane lipids of P4, P5, and P6 peroxisomes are shown. To calculate the initial rates of the LPAAT and PAP reactions, the [$^{14}$C]-labeled LPA, PA, and DAG were separated by TLC and quantified by autoradiography. To visualize nonradiolabeled PC, lipids were separated by TLC and detected using phosphomolybdic acid.

## The biosynthesis of PA and DAG in the peroxisomal membrane promotes the recruitment of Vps1p from the cytosol to the surface of the mature peroxisome

The *Saccharomyces cerevisiae* protein Vps1p is essential for peroxisome division (Hoepfner et al., 2001). Vps1p is a member of the dynamin protein superfamily of large GTPases that carry out a broad range of functions, including organelle division and fusion, budding of transport vesicles, and cytokinesis (Praefcke and McMahon, 2004). Akin to its *S. cerevisiae* counterpart, *Y. lipolytica* Vps1p is required for peroxisome division. In fact, lack of this protein resulted in a reduced number of greatly enlarged peroxisomes (Fig. S2, A and D). Like most peroxisomes of wild-type cells, the majority of peroxisomes of *vps1Δ* cells could be pelleted by centrifugation at 20,000 *g*. These 20,000-*g* pelletable peroxisomes of *vps1Δ* cells were very similar to mature peroxisomes purified from wild-type cells in regards to buoyant density, spectra of matrix and membrane proteins, and lipid composition of their membranes (unpublished data). Morphometric analysis of random electron sections further confirmed that lack of Vps1p impairs the ability of completely assembled peroxisomes to divide, resulting in fewer, but greatly enlarged, mature peroxisomes (Fig. S2, G and H).

*S. cerevisiae* Vps1p is mainly a cytosolic protein (Peters et al., 2004). It can also be found in a variety of cellular locations, including the Golgi, peroxisomes, and vacuoles (Hoepfner et al., 2001; Peters et al., 2004; Praefcke and McMahon, 2004). Likewise, most of *Y. lipolytica* Vps1p localized to the cytosol, whereas the minor portion of it was associated with both low-speed (20,000 *g*) and high-speed (200,000 *g*) pelletable organelles (Fig. S5 A, available at http://www.jcb.org/cgi/content/full/jcb.200609072/DC1). Using highly purified peroxisomal subforms of wild-type cells, we found that Vps1p was only present in division-competent mature peroxisomes (Fig. S5 B). In contrast, the division-incompetent immature peroxisomal vesicles P1–P5 lacked Vps1p (Fig. S5 B). The P6-associated form of Vps1p was solubilized completely by either 1 M NaCl or 0.1 M $Na_2CO_3$, pH 11.0, whereas the peroxisomal integral membrane protein Pex2p (Titorenko et al., 1996) was not (Fig. S5 C). Thus, Vps1p is a peripheral membrane protein.

Furthermore, Vps1p of mature peroxisomes was digested by trypsin even in the absence of the detergent Triton X-100, whereas the membrane-enclosed protein thiolase was resistant to digestion by external protease added to intact peroxisomes (Fig. S5 D). Altogether, these data imply that the conversion of P5 to P6 in wild-type cells is marked by the recruitment of Vps1p from the cytosol to the surface of mature peroxisomes.

Importantly, Vps1p was bound to division-competent mature peroxisomes of wild-type or *aox1Δ*, *aox2Δ*, and *aox3Δ* mutant strains (Fig. S5 E). In the membranes of mature peroxisomes of all these strains, LPA was converted to PA and DAG (Fig. 4). In contrast, Vps1p was not attached to mature peroxisomes of *aox4Δ*, *aox5Δ*, or *PEX16-TH* mutant strains (Fig. S5 E). All these strains are deficient in the division of mature peroxisomes (Guo et al., 2003), being unable to convert LPA to PA and DAG in the peroxisomal membrane (Figs. 1 and 4). These findings suggest that the recruitment of Vps1p from the cytosol to the surface of mature peroxisomes relies on the Pex16p/Aox-dependent biosynthesis of PA and DAG in their membranes.

### The recruitment of Vps1p to the peroxisomal membrane results in the formation of a multiprotein complex

To test whether Vps1p interacts with other components of the peroxisomal membrane, membrane proteins recovered after centrifugation of osmotically lysed mature peroxisomes of wild-type cells were treated with the thiol-cleavable cross-linker dithiobis(succinimidylpropionate) (DSP). These membrane proteins were immunoprecipitated with anti-Vps1p antibodies under denaturing, nonreducing conditions. The cross-linker was then cleaved with DTT, and the immunoprecipitated proteins were resolved by SDS-PAGE under reducing conditions, followed by silver staining. A cohort of proteins was specifically coimmunoprecipitated with Vps1p under these conditions (Fig. 6 A, lane 1), suggesting the existence of a Vps1p-containing complex on the outer face of the peroxisomal membrane. The following six components of this complex were identified by mass spectrometry: (1) Vps1p, a dynamin-like GTPase that is required for the division of mature peroxisomes (see the previous section); (2) Sla1p, a protein that regulates actin cytoskeleton organization and dynamics (Warren et al., 2002); (3) Abp1p, a protein that promotes F-actin assembly (Olazabal and Machesky, 2001); (4) Act1p, a structural constituent of actin cytoskeleton in yeast (Pruyne and Bretscher, 2000); (5) the peroxin Pex19p, a protein required for the import and/or membrane assembly of numerous PMPs (Subramani et al., 2000; Lambkin and Rachubinski, 2001); and (6) the peroxin Pex10p, an integral PMP required for peroxisomal matrix protein import (Subramani et al., 2000). Importantly, antibodies specific to Pex10p and Pex19p, the two components of the Vps1p-containing complex, immunoprecipitated the same set of DSP-treated PMPs as anti-Vps1p antibodies did (Fig. 6 A, compare lanes 1, 3, and 7). Thus, all Vps1p, Sla1p, Abp1p, Act1p, Pex19p, and Pex10p form a single multicomponent complex and do not compose several subcomplexes formed by the association of a bait protein (i.e., Vps1p, Pex10p, or Pex19p) with different subsets of interacting protein partners.

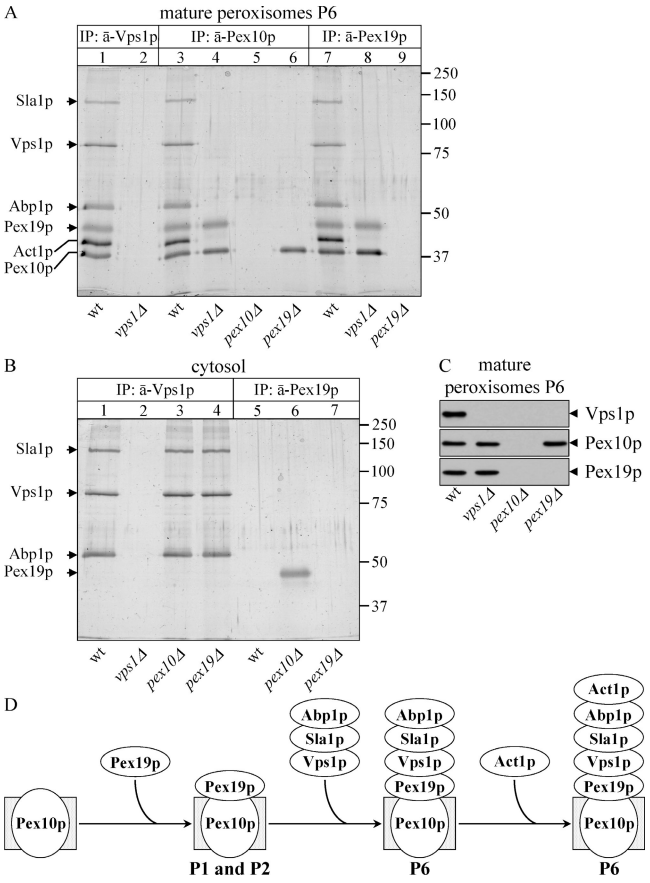


Figure 6. **A multiprotein complex that comprises a dynamin-like GTPase, three components of actin cytoskeleton, and two peroxins is assembled on the surface of the division-competent mature peroxisome.** (A) Highly purified mature peroxisomes of wild-type (wt) and mutant strains were osmotically lysed and subjected to centrifugation to yield supernatant (matrix proteins) and pellet (membrane proteins) fractions. Recovered membrane proteins were treated with the thiol-cleavable cross-linker DSP. These DSP-treated membrane proteins were immunoprecipitated with anti-Vps1p, anti-Pex10p, and anti-Pex19p antibodies under denaturing, nonreducing conditions. The cross-linker was then cleaved with DTT, and the immunoprecipitated proteins were resolved by SDS-PAGE under reducing conditions, followed by silver staining. (B) Wild-type and mutant cells were subjected to subcellular fractionation to yield the 200S (cytosolic) fraction. Cytosolic proteins were treated with DSP. These DSP-treated cytosolic proteins were subjected to immunoprecipitation with anti-Vps1p and anti-Pex19p antibodies under denaturing, nonreducing conditions. The cross-linker was then cleaved with DTT, and the immunoprecipitated proteins were resolved by SDS-PAGE under reducing conditions, followed by silver staining. Arrows in A and B indicate the positions of Sla1p, Vps1p, Abp1p, Pex19p, Act1p, and Pex10p, which were identified by mass spectrometry. (C) Equal quantities (20 μg) of protein from mature peroxisomes of wild-type and mutant strains were analyzed by immunoblotting with the indicated antibodies. (D) A model for the multistep assembly of the Act1p–Abp1p–Sla1p–Vps1p–Pex19p–Pex10p complex on the surface of mature peroxisomes.

The Pex10p and Pex19p components of the Vps1p-containing complex were associated with all six peroxisomal subforms, whereas Vps1p itself was attached only to mature peroxisomes P6 (Fig. S5 B). Furthermore, lack of either Pex10p or Pex19p abolished the recruitment of Vps1p from the cytosol to the membrane of P6 (Fig. 6 C). Moreover, in the absence of Vps1p, none of the actin cytoskeleton–related components of the Vps1p-containing complex, including Sla1p, Abp1p, and

Act1p, was bound to P6 (Fig. 6 A, lanes 4 and 8). Altogether, these findings imply that the Pex10p- and Pex19p-dependent recruitment of Vps1p from the cytosol to the surface of the mature peroxisome is mandatory for the attachment of Sla1p, Abp1p, and Act1p to this division-competent peroxisomal subform.

The Sla1p and Abp1p components of the Vps1p-containing complex, but not its Act1p component, coimmunoprecipitated with Vps1p from the DSP-treated cytosolic fractions of wild-type, *pex10Δ*, and *pex19Δ* cells (Fig. 6 B, lanes 1, 3, and 4). Act1p coimmunoprecipitated with Vps1p, Sla1p, and Abp1p only if all these proteins were attached to the surface of mature peroxisomes (Fig. 6 A, lanes 1, 3, and 7). Hence, Vps1p, Sla1p, and Abp1p initially form a complex in the cytosol. This complex is then targeted from the cytosol to the surface of mature peroxisomes. Only after its binding to mature peroxisomes, the Vps1p–Sla1p–Abp1p complex is able to promote the attachment of Act1p to the peroxisomal membrane. Akin to Vps1p (see the previous section), each of the two other components of the Vps1p–Sla1p–Abp1p complex is required for peroxisome division. In fact, lack of either Sla1p or Abp1p resulted in a reduced number of greatly enlarged peroxisomes (Fig. S2, E–H).

The Pex10p component of the Vps1p-containing complex is an integral PMP that could not be stripped off the peroxisomal membrane by either 1 M NaCl or 0.1 M $Na_2CO_3$, pH 11.0 (Fig. S5 C). On the contrary, its Pex19p component is a peripheral membrane protein on the outer face of peroxisomes that could be solubilized by either 1 M NaCl or 0.1 M $Na_2CO_3$, pH 11.0, and was sensitive to digestion by external protease added to intact peroxisomes (Fig. S5, C and D). Pex10p and Pex19p form a complex in the membrane of mature peroxisomes (Fig. 6 A, lanes 4 and 8) and of immature peroxisomal vesicles P1–P5 (not depicted). Thus, the Pex10p–Pex19p complex assembles in the peroxisomal membrane during the initial steps of the peroxisome assembly pathway. The attachment of Pex19p to the peroxisomal membrane requires Pex10p, as lack of Pex10p abolished the recruitment of Pex19p from the cytosol to the peroxisome (Fig. 6 C). Of note, Pex19p that was accumulated in the cytosol of *pex10Δ* cells did not coimmunoprecipitate with Vps1p, Sla1p, Abp1p, or Act1p (Fig. 6 B, lane 6). Furthermore, the Vps1p–Sla1p–Abp1p complex could be formed even in the cytosol of *pex19Δ* cells (Fig. 6 B, lane 4). These findings support the notion that, although cytosolic Pex19p is not required for the assembly of the Vps1p–Sla1p–Abp1p complex before its recruitment to the membrane, the membrane-bound form of Pex19p is mandatory for the attachment of the preformed Vps1p–Sla1p–Abp1p complex to the surface of mature peroxisomes.

In summary, our data suggest that the assembly of the Vps1p–Sla1p–Abp1p complex in the cytosol precedes its attachment to the surface of division-competent mature peroxisomes P6 (Fig. 6 D). The Vps1p–Sla1p–Abp1p complex binds to P6 by interacting with Pex19p, a component of the Pex10p–Pex19p complex that is formed in the peroxisomal membrane during the earliest steps of peroxisome assembly and maturation. Only after it has been attached to the membrane of P6 is the Vps1p–Sla1p–Abp1p complex able to interact with Act1p, thereby promoting the recruitment of actin to the surface of these division-competent peroxisomes.

## Discussion

This study and our published data (Guo et al., 2003) suggest the following model for peroxisome division in *Y. lipolytica* (Fig. 7). In immature peroxisomal vesicles P1–P5, Pex16p binds LPA in the lumenal leaflet of the peroxisomal membrane. The binding of Pex16p to LPA prevents the biosynthesis of PA and DAG in a two-step pathway, which includes two consecutive enzymatic reactions catalyzed by Slc1p (LPAAT) and Dpp1p (PAP; Fig. 1 D).

The stepwise import of distinct subsets of matrix proteins into immature peroxisomal vesicles P1–P5 provides them with an increasing fraction of the matrix proteins present in mature peroxisomes. The increase in the total mass of matrix proteins above a critical level, which occurs only inside mature peroxisomes, causes the redistribution of Aox from the matrix to the membrane and its subsequent binding to Pex16p. This, in turn, greatly decreases the affinity between Pex16p and LPA, thereby allowing LPA to enter the two-step biosynthetic pathway leading to the formation of PA and DAG. The glycerophospholipid PC, which is transferred to the peroxisomal membrane from the P3- and P4-associated subcompartment of the ER, activates both LPAAT and PAP. The resulting accumulation of PA and DAG in the lumenal leaflet of the membrane of mature peroxisomes triggers a cascade of events ultimately leading to peroxisome division. This cascade of events is initiated by the spontaneous flipping of DAG, which is known for its very fast transbilayer translocation, between the two membrane leaflets. The movement of DAG, a particularly potent cone-shaped inducer of membrane bending, from the lumenal to the cytosolic leaflet of the membrane bilayer coincides with the translocation of the glycerophospholipid PS in the opposite direction. This bidirectional movement of DAG and PS generates a lipid imbalance across the bilayer, which may promote the destabilization and bending of the membrane. The biosynthesis of PA and DAG in the membrane of mature peroxisomes and, perhaps, the bending of the membrane because of the bidirectional transbilayer movement of DAG and PS promote the docking of the Vps1p–Sla1p–Abp1p complex to the surface of mature peroxisomes. This preassembled in the cytosol protein complex binds to mature peroxisomes by interacting with the peroxin Pex19p. Pex19p is a component of the Pex10p–Pex19p complex that is formed in the peroxisomal membrane during the earliest steps of peroxisome assembly (Fig. 6 D). After its attachment to the peroxisomal membrane, the Vps1p–Sla1p–Abp1p complex interacts with Act1p, thereby recruiting this structural constituent of actin cytoskeleton to the surface of mature peroxisomes. The subsequent fission of the peroxisomal membrane leads to peroxisome division.

It remains to be established how exactly Vps1p promotes peroxisome division. Initially, this dynamin-like GTPase interacts in the cytosol with Sla1p and Abp1p. Vps1p then functions in the attachment of the Vps1p–Sla1p–Abp1p protein complex to its docking factor Pex19p on the surface of mature peroxisomes,

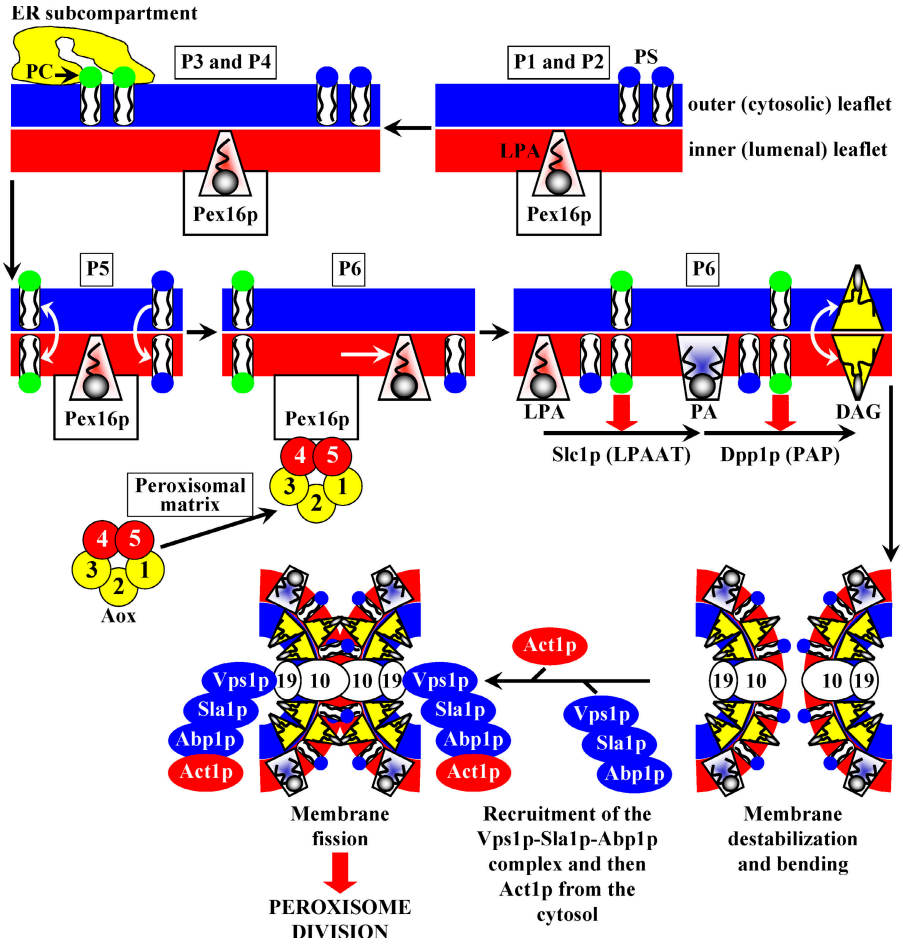


Figure 7. **The Pex16p- and Aox-dependent intraperoxisomal signaling cascade drives the division of mature peroxisomes P6 by promoting the stepwise remodeling of lipid and protein composition of the peroxisomal membrane.** The peroxisome becomes competent for division only after it acquires the complete set of matrix proteins involved in lipid metabolism. Overloading the peroxisome with matrix proteins promotes the relocation of Aox, an enzyme of fatty acid β-oxidation, from the matrix to the membrane. The binding of Aox to Pex16p, a membrane-associated peroxin required for peroxisome biogenesis, activates the biosynthesis and transbilayer movement of a distinct set of membrane lipids. The resulting remodeling of the lipid repertoire of the membrane bilayer initiates the stepwise assembly of a multicomponent protein complex on the surface of the mature peroxisome. This newly assembled protein complex carries out membrane fission, thereby executing the terminal step of peroxisome division.

thereby promoting the subsequent recruitment of actin to the membrane of division-competent peroxisomes. Therefore, it seems unlikely that Vps1p acts only as a mechanochemical enzyme (Praefcke and McMahon, 2004) whose GTPase activity provides the mechanical force required for membrane fission in the constricted neck. Our data suggest that this dynamin-like protein may rather function as a regulatory GTPase (Newmyer et al., 2003) whose GTP-bound form promotes the multistep assembly of the membrane fission machinery, initially in the cytosol and then on the surface of division-competent mature peroxisomes. This machinery includes the Sla1p, Abp1p, and Act1p components of actin cytoskeleton. The mechanism by which actin cytoskeleton regulates the terminal step of peroxisome division is currently being investigated.

Similar to mitotic Golgi fragmentation (Shorter and Warren, 2002; Corda et al., 2006) and mitochondrial division during apoptosis (Youle and Karbowski, 2005), peroxisome division is served by a protein team that is assembled on the peroxisomal surface in a stepwise fashion. The multicomponent protein machineries serving Golgi fragmentation and mitochondrial division are assembled in response to extraorganellar stimuli (Shorter and Warren, 2002; Youle and Karbowski, 2005). In contrast, the protein team that executes peroxisome division undergoes multistep assembly in response to an intraperoxisomal signaling cascade (Fig. 7). Although this Pex16p- and Aox-dependent signaling cascade is turned off inside immature peroxisomal vesicles, it is activated inside mature peroxisomes. Thus, it seems likely that the intraperoxisomal cascade for fine-tuning the fission of peroxisomal membrane is an intrinsic feature of the multistep peroxisome biogenesis program. Perhaps this program has evolved to separate the dramatic changes in the composition and architectural design of the membrane bilayer, all of which occur during peroxisome division, from the process of protein translocation across this bilayer, which takes place during peroxisome assembly. One of the benefits of using such strategy for the temporal separation of the processes of peroxisome assembly and division is that some of the membrane components can efficiently function in both processes. In fact, the peroxins Pex10p and Pex19p, known for their essential role in peroxisomal import of numerous matrix proteins and PMPs (Subramani et al., 2000), are also required for the assembly of the peroxisome division machinery on the surface of mature peroxisomes (Fig. 6 D).

Our findings support the notion that a distinct set of lipid metabolic pathways operating in organellar membranes and specific changes in the distribution of some lipids across the membrane bilayers provide a driving force for organelle division (Bankaitis, 2002; Farsad and De Camilli, 2003; Shemesh et al., 2003; Behnia and Munro, 2005; Diaz Anel and Malhotra, 2005; McMahon and Gallop, 2005; Corda et al., 2006). It is tempting to speculate that, after its spontaneous flipping between the two leaflets of the peroxisomal membrane (Fig. 7),

DAG undergoes the selective enrichment in distinct lipid domains that facilitate membrane fission through coordinated changes in local membrane curvature, initiate the assembly of the Vps1p-containing protein complexes on the surface of peroxisomes, and promote the clustering of these protein complexes at the membrane fission site. A challenge for the future will be to define the spatial distribution of DAG and Vps1p-containing protein complexes in the membrane of division-competent mature peroxisomes.

## Materials and methods

**Strains and reagents**

The *Y. lipolytica* wild-type strain *P01d* (Wang et al., 1999); the mutant strains *pex2Δ* (Titorenko et al., 1996), *pex19Δ* (Lambkin and Rachubinski, 2001), *pex16Δ*, and *PEX16-TH* (Eitzen et al., 1997); the single *AOX* gene knock-out strains (Wang et al., 1999); and the media, growth conditions, and genetic techniques for *Y. lipolytica* (Titorenko et al., 1998) have been previously described. Targeted integrative disruption of the *ABP1*, *DPP1*, *PEX10*, *SLA1*, *SLC1*, and *VPS01* genes was performed with the *URA3* gene of *Y. lipolytica*, using a previously described modification of the sticky-end polymerase chain reaction procedure (Wang et al., 1999). J.-M. Nicaud (Laboratoire de Microbiologie et de Génétique Moléculaire, Thiverval-Grignon, France) provided the *pex10Δ* and *vps1Δ* mutant strains. Antibodies to Pex2p (Titorenko et al., 1996), Pex16p (Titorenko et al., 2000), Pex19p (Lambkin and Rachubinski, 2001), and thiolase (Titorenko et al., 2000) have been previously described and were provided by R.A. Rachubinski (University of Alberta, Edmonton, Canada). Monospecific antibodies to Dpp1p, Pex10p, Slc1p, and Vps1p were raised in rabbit against their peptides GAPRPDMLARCRPMSWMRP, CRQGVREQNLLPIR, GRIFPQYC-SVTAKKALKWYP, and MDKELISTVNKLQDALA, respectively. Purification of the DAG-binding C1b domain of protein kinase C (Johnson et al., 2000) and its labeling with the fluorophore Alexa Fluor 488 (Fratti et al., 2004) were performed as described previously. The GST-C1B vector was provided by A.C. Newton (University of California at San Diego, La Jolla, CA). SDS-PAGE and immunoblotting (Titorenko et al., 1998) were performed as described. Cholic acid (sodium salt), ergosterol, hydroxylapatite, n-OG, palmitoyl-CoA agarose, and Triton X-100 were purchased from Sigma-Aldrich. PIP Strips were obtained from Echelon Biosciences. Alexa Fluor 488 signal-amplification kit for fluorescein-conjugated probes was purchased from Invitrogen. Monoclonal anti-PS antibody was purchased from Upstate Biotechnology. Fluorescein-conjugated goat anti–rabbit IgG antibodies and fluorescein-conjugated goat anti–mouse IgM antibodies were obtained from Jackson ImmunoResearch Laboratories. *N*-palmitoyl-D-*erythro*-sphingosine (ceramide), 1,2-dioleoyl-*sn*-glycerol (DAG), 1,2-dioleoyl-*sn*-glycero-3-phosphate (PA), 1,2-dioleoyl-*sn*-glycero-3-phosphocholine (PC), 1-oleoyl-2-hydroxy-*sn*-glycero-3-phosphate (LPA), 1,2-dioleoyl-*sn*-glycero-3-phosphoethanolamine (PE), L-α-phosphatidylinositol (PI), and 1,2-dioleoyl-*sn*-glycero-3-(phospho-L-serine) (PS) were obtained from Avanti Polar Lipids, Inc. [$C^{14}$]-labeled lipids, HiTrap Blue HP, Resource Q, Resource S, and Superose 12 were obtained from GE Healthcare.

**Subcellular fractionation and isolation of organelles**

The initial step in the subcellular fractionation of oleic acid-grown cells included the differential centrifugation of lysed and homogenized spheroplasts at 1,000 *g* for 10 min at 4°C in a JS13.1 rotor (Beckman Coulter) to yield a postnuclear supernatant fraction. The postnuclear supernatant fraction was further subjected to differential centrifugation at 20,000 *g* for 30 min at 4°C in a JS13.1 rotor to yield pellet (20KgP) and supernatant (20KgS) fractions. The 20KgS fraction was further subfractionated by differential centrifugation at 200,000 *g* for 1 h at 4°C in a TLA110 rotor (Beckman Coulter) to yield pellet (200KgP) and supernatant (200KgS) fractions.

To purify immature peroxisomal vesicles P1–P5, the 200KgP subcellular fraction was subjected to centrifugation on a discontinuous sucrose (18, 25, 30, 35, 40, and 53%; wt/wt) gradient at 120,000 *g* for 18 h at 4°C in a SW28 rotor (Beckman Coulter). 36 fractions of 1 ml each were collected. Different subforms of immature peroxisomal vesicles peaked at densities of 1.18 g/$cm^3$ (fraction 5; P5), 1.14 g/$cm^3$ (fraction 15; P3 + P4), 1.11 g/$cm^3$ (fraction 23; P1), and 1.09 g/$cm^3$ (fraction 30; P2) were recovered (Titorenko et al., 2000). The peak fractions containing immature peroxisomal vesicles P1, P2, P3 + P4, and P5 were recovered, and 4 vol of 0.5 M sucrose in buffer H (5 mM MES, pH 5.5, 1 mM KCl, 0.5 mM EDTA, 0.1% ethanol, and 1× protease inhibitor cocktail [Titorenko et al., 1998]) were added to each of them. Peroxisomes were pelleted onto a 150-μl cushion of 2 M sucrose in buffer H by centrifugation at 200,000 *g* for 20 min at 4°C in a TLA110 rotor. Individual pellets of different subforms of immature peroxisomal vesicles were resuspended in 3 ml of 50% (wt/wt) sucrose in buffer H.

For purification of immature peroxisomal vesicles P1 and P2, pellets of P1 and P2 resuspended in 50% (wt/wt) sucrose in buffer H were overlaid with 30, 28, 26, 24, 22, and 10% sucrose (all wt/wt in buffer H). After centrifugation at 120,000 *g* for 18 h at 4°C in a SW28 rotor, 18 fractions of 2 ml each were collected. P1 and P2 were pelleted, resuspended, and subjected to a second flotation on the same multistep sucrose gradient. Gradients were fractionated into 2-ml fractions, and P1 and P2 were recovered (Titorenko et al., 2000) and used for biochemical analyses.

For purification of immature peroxisomal vesicles P3 and P4, pellets of P3 and P4 resuspended in 50% (wt/wt) sucrose in buffer H were overlaid with 38, 35, 33, and 20% sucrose (all wt/wt in buffer H). After centrifugation at 120,000 *g* for 18 h at 4°C in a SW28 rotor, 18 fractions of 2 ml each were collected. P3 and P4 were pelleted, resuspended in 3 ml of 50% (wt/wt) sucrose in buffer HE (20 mM MES, pH 5.5, 20 mM EDTA, and 0.1% ethanol), overlaid with 39, 37, 35, 33, and 20% sucrose (all wt/wt in buffer HE), and subjected to centrifugation as described. Gradients were fractionated into 2-ml fractions, and P3 and P4 were recovered and pelleted. After resuspension in 3 ml of 50% (wt/wt) sucrose in buffer H, P3 and P4 were again subjected to flotation on the second multistep sucrose gradient described. Gradients were fractionated into 2-ml fractions, and P3 and P4 were recovered (Titorenko et al., 2000) and used for biochemical analyses.

Highly purified mature peroxisomes P6 were isolated from the 20KgP subcellular fraction by isopycnic centrifugation on a discontinuous sucrose gradient as described previously (Titorenko et al., 1996). 4 vol of 0.5 M sucrose in buffer H were added to the peak peroxisomal fraction 4 recovered after isopycnic centrifugation on a discontinuous sucrose gradient. Peroxisomes were sedimented through a 150-μl cushion of 2 M sucrose in buffer H by centrifugation at 200,000 *g* for 20 min at 4°C in a TLA110 rotor. The resultant pellet of mature peroxisomes P6 was resuspended in buffer H containing 1 M sorbitol and was subjected to further centrifugation on a linear 20–60% (wt/wt) sucrose gradient (in buffer H) at 197,000 *g* for 18 h at 4°C in a SW41Ti rotor (Beckman Coulter). Peak peroxisomal fraction 5 equilibrating at a density of 1.21 g/$cm^3$ was recovered, and peroxisomes were sedimented through a 150-μl cushion of 2 M sucrose in buffer H by centrifugation at 200,000 *g* for 20 min at 4°C in a TLA110 rotor. Pellet of mature peroxisomes P6 was resuspended in 55% (wt/wt) sucrose in buffer H, overlaid with 50, 45, 40, 30, and 20% sucrose (all wt/wt in buffer H), and subjected to centrifugation at 120,000 *g* for 18 h at 4°C in a SW28 rotor. 18 gradient fractions of 2 ml each were collected. Peak peroxisomal fraction 11 equilibrating at a density of 1.21 g/$cm^3$ was recovered (Titorenko et al., 2000) and used for biochemical analyses.

The free form of the ER (Titorenko et al., 1996) and the P3- and P4-associated subcompartment of the ER (Titorenko et al., 2000) were purified from *Y. lipolytica* cells as described previously. Subcellular fractionation of *S. cerevisiae* cells grown in glucose-containing YEPD medium and isolation of functional ER membranes were performed according to established procedures (Rieder and Emr, 2000).

**Peroxisome subfractionation and extraction**

Highly purified peroxisomes were lysed by the addition of 10 vol of ice-cold LB buffer (20 mM Hepes-KOH, pH 8.0, 50 mM NaCl, and 1× protease inhibitor cocktail), followed by incubation on ice for 30 min with occasional agitation. The suspension was centrifuged at 200,000 *g* for 20 min at 4°C in a TLA110 rotor. The pellet of membranes recovered after centrifugation of osmotically lysed peroxisomes was resuspended in ice-cold EB buffer (10 mM Hepes-KOH, pH 8.0, 5 mM EDTA, and 1× protease inhibitor cocktail) to a final concentration of 1.0 mg/ml. Equal aliquots of the suspension of membranes were then exposed to 1 M NaCl, 0.1 M $Na_2CO_3$, pH 11.0, or 0.5% (vol/vol) Triton X-100 (Titorenko et al., 1998). After incubation on ice for 30 min with occasional agitation, the samples were subjected to centrifugation at 100,000 *g* for 30 min at 4°C in a TLA110 rotor. Equal portions of the pellet and supernatant fractions were analyzed by SDS-PAGE, followed by immunoblotting.

**Protease protection analysis**

The pellet of highly purified mature peroxisomes was gently resuspended in ice-cold PPB buffer (5 mM MES, pH 5.5, 1 M sorbitol, 1 mM KCl, and 0.5 mM EDTA). Equal aliquots (10 or 20 μg of total protein) of these

peroxisomes were incubated with 0, 5, 10, or 50 μg trypsin for 30 min on ice, either in the presence or absence of Triton X-100 at 0.5% (vol/vol) final concentration. The reaction was terminated by the addition of trichloroacetic acid to 10% final concentration. The protein precipitates were washed with ice-cold 80% (vol/vol) acetone, and equivalent fractions of each reaction were subjected to SDS-PAGE and immunoblotting.

**Lipid analyses**

Highly purified peroxisomes were lysed by the addition of 10 vol of ice-cold LB buffer, followed by incubation on ice for 30 min with occasional agitation. The suspension was centrifuged at 200,000 *g* for 20 min at 4°C in a TLA110 rotor. The recovered pellet of membranes that contained 1 mg of membrane protein was resuspended in 1.0 ml of chloroform/methanol (1:1; vol/vol). After incubation on ice for 15 min with occasional agitation, samples were subjected to centrifugation at 20,000 *g* for 15 min at 4°C. The chloroform phase was separated and dried under nitrogen. The lipid film was dissolved in 100 μl of chloroform (for the analysis of DAG, ergosterol, and ceramide) or 100 μl of chloroform/methanol (1:1 [vol/vol]; for the analysis of PE, PA, PC, PI, PS, and LPA). 25 μl of each sample were spotted on 60-Å silica gel plates for TLC (Whatman). The lipids were developed in the following solvent systems: chloroform/acetone (4.6:0.4 [vol/vol]; for the analysis of DAG, ergosterol, and ceramide) and chloroform/methanol/water (65:25:4 [vol/vol]; for the analysis of PE, PA, PC, PI, PS, and LPA). All lipids were detected using 5% phosphomolybdic acid in ethanol and visualized by heating for 30 min at 110°C. Lipids were quantitated by densitometric analysis of TLC plates as described previously (Fried and Sherma, 1999), using lipid standards in the 0.1–0.5 μg range for calibration.

For monitoring enzymatic activities of LPAAT and PAP, highly purified peroxisomes were lysed by the addition of 10 vol of ice-cold LB buffer, followed by incubation on ice for 30 min with occasional agitation. The suspension was centrifuged at 200,000 *g* for 20 min at 4°C in a TLA110 rotor. The pellet of membranes recovered after centrifugation of osmotically lysed peroxisomes was resuspended in ice-cold buffer R (20 mM MES-KOH, pH 6.0, 150 mM NaCl, 5 mM DTT, and 10% glycerol) containing 1% (wt/vol) n-OG. After incubation on ice for 20 min with occasional agitation, the sample of detergent-solubilized PMPs was subjected to centrifugation at 100,000 *g* for 20 min at 4°C in a TLA110 rotor. The resulting supernatant of solubilized PMPs was depleted of Pex16p by immunoaffinity chromatography under native conditions using anti-Pex16p antibodies covalently linked to protein A–Sepharose (Szilard et al., 1995). For the reconstitution of peroxisomal liposomes carrying Pex16p, detergent-solubilized PMPs immunodepleted of Pex16p were supplemented with Pex16p, which was purified from membranes of osmotically lysed immature peroxisomal vesicles P1 by immunoaffinity chromatography under native conditions using anti-Pex16p antibodies covalently linked to protein A–Sepharose (Szilard et al., 1995). After elution with buffer E (20 mM Hepes-KOH, pH 7.5, 250 mM $MgCl_2$, 5 mM DTT, and 10% glycerol) containing 1% (wt/vol) n-OG, purified Pex16p was dialyzed against buffer R supplemented with 1% (wt/vol) n-OG. For the reconstitution of peroxisomal liposomes lacking Pex16p, detergent-solubilized PMPs immunodepleted of Pex16p were supplemented only with buffer R containing 1% (wt/vol) n-OG. Detergent-solubilized PMPs immunodepleted of Pex16p and either supplemented or not supplemented with purified Pex16p in buffer R containing 1% (wt/vol) n-OG were then added to the films of unlabeled lipids, which were initially extracted from the membranes of highly purified peroxisomes using chloroform/methanol (1:1; vol/vol) and then dried down by a gentle stream of nitrogen. The lipid films were dissolved by gentle agitation for 20 min at room temperature. For monitoring LPAAT activity, the unlabeled lipids, which were extracted from the membranes of highly purified peroxisomes using chloroform/methanol (1:1; vol/vol), were supplemented with [$^{14}$C]-labeled LPA and unlabeled oleoyl-CoA (a cosubstrate of LPAAT) dissolved in chloroform/methanol (1:1; vol/vol). The mix of unlabeled membrane lipids and [$^{14}$C]-labeled LPA was then dried down by a gentle stream of nitrogen. For monitoring PAP activity, the unlabeled lipids, which were extracted from the membranes of highly purified peroxisomes using chloroform/methanol (1:1; vol/vol), were supplemented with [$^{14}$C]-labeled PA dissolved in chloroform/methanol (1:1; vol/vol). The mix of unlabeled membrane lipids and [$^{14}$C]-labeled PA was then dried down by a gentle stream of nitrogen. For evaluating the positive effect of PC on LPAAT and PAP, equal aliquots of unlabeled lipids extracted from the membranes of highly purified peroxisomes using chloroform/methanol (1:1; vol/vol) were first mixed with an appropriate [$^{14}$C]-labeled lipid substrate of LPAAT or PAP in chloroform/methanol (1:1; vol/vol) and were then supplemented with various quantities of PC dissolved in chloroform/methanol (1:1; vol/vol). The mix of unlabeled membrane lipids, a [$^{14}$C]-labeled lipid substrate, and unlabeled PC was then dried down by a gentle stream of nitrogen. The lipid films were finally dissolved by gentle agitation for 20 min at room temperature in buffer R containing detergent-solubilized PMPs, immunodepleted or not immunodepleted of Pex16p, in 1% (wt/vol) n-OG.

To dilute the detergent n-OG below its critical micellar concentration, thereby promoting the formation of peroxisomal liposomes, 3 vol of buffer D (20 mM MES-KOH, pH 6.0, and 150 mM NaCl) was added to the mixture of detergent-solubilized PMPs, and membrane lipids were dissolved in buffer R containing 1% (wt/vol) n-OG. To remove the detergent, the samples were dialyzed in a Tube-O-Dialyzer (7.5-kD cutoff; Chemicon) against buffer D containing 0.1% Biobeads SM2 (Bio-Rad Laboratories). After overnight dialysis at 4°C, samples were transferred to the bottom of ultraclear centrifuge tubes (Beckman Coulter) and supplemented with 4 vol of 65% (wt/wt) sucrose in buffer D in order to adjust the sucrose concentration of the samples to 52% (wt/wt). Samples were overlaid with 40% and then with 20% sucrose (both wt/wt in buffer D) and, lastly, with buffer D alone. After centrifugation at 200,000 *g* for 18 h at 4°C in a SW50.1 rotor (Beckman Coulter), 18 fractions of 275 μl each were collected. Peroxisomal liposomes were recovered at the 40%/20% sucrose interface.

The recovered peroxisomal liposomes were transferred from ice to 26°C. Samples were taken at the indicated times after the transfer. Lipids were extracted from the membrane and analyzed by TLC. To calculate the initial rates of the LPAAT and PAP reactions, the [$^{14}$C]-labeled LPA, PA, and DAG were separated by TLC and quantified by autoradiography.

To evaluate the transbilayer distribution of DAG and PS in the membrane bilayers of different peroxisomal subforms, the suspension of highly purified peroxisomes in ice-cold H250S buffer (5 mM MES-KOH, pH 5.5, 250 mM sorbitol, 1 mM KCl, 0.5 mM EDTA, and 1× protease inhibitor cocktail) at 1 mg protein/ml was divided into two equal aliquots. One aliquot remained untreated, whereas peroxisomal vesicles in the other aliquot were lysed by the addition of 10 vol of ice-cold LB buffer, followed by incubation on ice for 30 min with occasional agitation. The suspension of lysed peroxisomes was divided into two equal aliquots. One aliquot was dialyzed in a Tube-O-Dialyzer (7.5-kD cutoff) against buffer MR (10 mM MES/KOH, pH 5.5, 1 mM KCl, and 0.5 mM EDTA) containing 250 mM sorbitol. The suspension of lysed peroxisomes in the other aliquot was dialyzed in a Tube-O-Dialyzer (7.5-kD cutoff) against buffer HR (10 mM Hepes/KOH, pH 7.5, 1 mM KCl, and 0.5 mM EDTA) containing 250 mM sorbitol. After overnight dialysis at 4°C, resealed peroxisomes RPA that were formed in the aliquot dialyzed against buffer MR containing 250 mM sorbitol and resealed peroxisomes RPB that were formed in the aliquot dialyzed against buffer HR containing 250 mM sorbitol were pelleted onto a 150-μl cushion of 2 M sucrose in buffer MR or HR, respectively, by centrifugation at 100,000 *g* for 20 min at 4°C in a TLA110 rotor. Individual pellets of RPA and RPB were resuspended in 500 μl of 50% (wt/wt) sucrose in buffer MR or HR, respectively. The sample containing RPA was overlaid with 1.5 ml of 45% sucrose, 1 ml of 40% sucrose, 1 ml of 25% sucrose, and 1 ml of 10% sucrose (all wt/wt in buffer MR). The sample containing RPB was overlaid with 1.5 ml of 45% sucrose, 1 ml of 40% sucrose, 1 ml of 25% sucrose, and 1 ml of 10% sucrose (all wt/wt in buffer HR). Both samples were subjected to centrifugation at 200,000 *g* for 18 h at 4°C in a SW50.1 rotor. Nine fractions of 555 μl each were collected. Resealed peroxisomes RPA and RPB floated to low density during centrifugation in the sucrose density gradient. Proteins from equal volumes of gradient fractions were analyzed by immunoblotting with antibodies to Pex16p and Pex19p. Equal volumes of gradient fractions were also subjected to lipid extraction, which was followed by TLC and visualization of lipids.

Resealed peroxisomes RPA and RPB, which were recovered in the peak fractions of the flotation gradients, and a highly purified subform of the intact peroxisomes from which these two types of resealed peroxisomes were formed, were used to evaluate the orientation in which the membranes delimiting RPA and RPB were resealed. RPA and RPB were pelleted onto a 150-μl cushion of 2 M sucrose in buffer MR or HR, respectively, by centrifugation at 100,000 *g* for 20 min at 4°C in a TLA110 rotor. Intact peroxisomes were pelleted onto a 150-μl cushion of 2 M sucrose in buffer H by centrifugation at 100,000 *g* for 20 min at 4°C in a TLA110 rotor. Individual pellets of RPA, RPB, and intact peroxisomes were resuspended in ice-cold buffer H at 1 mg protein/ml. Serial dilutions of RPA, RPB, and intact peroxisomes in the range of 10–50 μg protein/ml were made in ice-cold buffer H. Anti-Pex16p rabbit IgG or anti-Pex19p rabbit IgG were added to concentrations 4 and 5 μg/ml, respectively. After incubation for 30 min on ice, samples were subjected to centrifugation at 100,000 *g* for 10 min at 4°C in a TLA110 rotor. The pellets were resuspended in 200 μl of ice-cold buffer H and supplemented with fluorescein-conjugated goat

anti–rabbit IgG. After incubation for 30 min on ice, samples were subjected to centrifugation at 100,000 *g* for 10 min at 4°C in a TLA110 rotor. The pellets were resuspended in 200 μl of ice-cold buffer H and supplemented with Alexa Fluor 488 goat anti-fluorescein/Oregon green IgG at 15 μg/ml. After incubation for 30 min on ice, samples were subjected to centrifugation at 100,000 *g* for 10 min at 4°C in a TLA110 rotor. The pellets were resuspended in 200 μl of ice-cold buffer H and supplemented with Alexa Fluor 488 chicken anti–goat IgG at 20 μg/ml. After incubation for 30 min on ice, samples were subjected to centrifugation at 100,000 *g* for 10 min at 4°C in a TLA110 rotor. The pellets were resuspended in 200 μl of ice-cold buffer H and placed into the wells of a 96-well microplate. The fluorescence of samples was measured using the Victor 2 multilabel microplate fluorescence reader (Wallac) with filters set at 485 (±7.5) nm (excitation) and 510 (±5) nm (emission). Controls were made for each dilution of RPA, RPB, and intact peroxisomes. The controls included normal rabbit IgG at 4 or 5 μg/ml added instead of anti-Pex16p rabbit IgG or anti-Pex19p rabbit IgG, respectively. Background fluorescence, which was due to the nonspecific binding of rabbit IgG and/or fluorescein- or Alexa Fluor 488–labeled antibodies to the peroxisomal membrane, was subtracted.

In intact peroxisomes, Pex19p is a peripheral membrane protein that resides on the outer (cytosolic) face of the peroxisome (Fig. 2 D and Fig. S5, C and D). Because this protein is attached to the surface of intact peroxisomes, it is accessible to anti-Pex19p IgG exogenously added to these peroxisomes (Fig. S3 D, right). Importantly, the membranes of intact peroxisomes, RPA, and RPB are not permeable to the exogenously added IgG molecules. In fact, none of Pex16p, a peripheral membrane protein residing on the inner (lumenal) face of the peroxisome, in intact peroxisomes and only a minor portion of this protein in RPA was accessible to anti-Pex16p IgG (Fig. S3 D, left). The observed accessibility of the RPB-associated form of Pex16p to anti-Pex16p IgG was due to the inside-out orientation of the membrane delimiting most of the RPB species formed during peroxisome resealing. In addition, although the levels of Pex19p, a peripheral membrane protein residing on the peroxisomal surface, in intact peroxisomes, RPA, and RPB were very similar to each other (Fig. S3 B), only a minor portion of Pex19p in the mostly inside-out–oriented RPB species was accessible to anti-Pex19p IgG (Fig. S3 D, right). Altogether, these findings imply that, if the fluorescence for RPA ($F_{RPA}$)/fluorescence for intact peroxisomes ($F_{IP}$) or fluorescence for RPB ($F_{RPB}$)/fluorescence for intact peroxisomes ($F_{IP}$) ratio is calculated for Pex19p, it is equal to the fraction of the total pool of Pex19p that resides on the outer (cytosolic) face of those RPA or RPB species whose delimiting membranes acquired the outside-out orientation during their resealing. At the same time, the $(F_{IP} - F_{RPA})/F_{IP}$ or $(F_{IP} - F_{RPB})/F_{IP}$ ratio, if calculated for Pex19p, equals the fraction of Pex19p that resides on the inner (lumenal) face of those RPA or RPB species whose delimiting membranes acquired the inside-out orientation during their resealing. Hence, the $F_{RPA}/F_{IP}$ or $F_{RPB}/F_{IP}$ ratio for Pex19p is equal to the fraction of those RPA or RPB species that are present in the outside-out orientation ($n^{oo}{}_{RPA}$ and $n^{oo}{}_{RPB}$, respectively). Moreover, the $(F_{IP} - F_{RPA})/F_{IP}$ or $(F_{IP} - F_{RPB})/F_{IP}$ ratio for Pex19p equals the fraction of those RPA or RPB species that were resealed in the inside-out orientation ($n^{io}{}_{RPA}$ and $n^{io}{}_{RPB}$, respectively).

Resealed peroxisomes RPA and RPB, which were recovered in the peak fractions of the flotation gradients, and a highly purified subform of the intact peroxisomes from which these two types of resealed peroxisomes were formed, were used to calculate the percentage of DAG and PS residing in the cytosolic and lumenal leaflets of the membrane bilayers in different peroxisomal subforms. RPA and RPB were pelleted onto a 150-μl cushion of 2 M sucrose in buffer MR or HR, respectively, by centrifugation at 100,000 *g* for 20 min at 4°C in a TLA110 rotor. Intact peroxisomes were pelleted onto a 150-μl cushion of 2 M sucrose in buffer H by centrifugation at 100,000 *g* for 20 min at 4°C in a TLA110 rotor. Individual pellets of RPA, RPB, and intact peroxisomes were resuspended in ice-cold buffer H at 1 mg protein/ml. Serial dilutions of RPA, RPB, and intact peroxisomes in the range of 10–50 μg protein/ml were made in ice-cold buffer H. The DAG-binding C1b domain of protein kinase C labeled with the fluorophore Alexa Fluor 488 or anti-PS mouse IgM were added to concentrations 5 and 1 μg/ml, respectively. After incubation for 30 min on ice, samples were subjected to centrifugation at 100,000 *g* for 10 min at 4°C in a TLA110 rotor. For samples that were exposed to Alexa Fluor 488–tagged C1b domain, the pellets were resuspended in 200 μl of ice-cold buffer H and placed into the wells of a 96-well microplate. The fluorescence of these samples was measured using the Victor 2 multilabel microplate fluorescence reader with filters set at 485 (±7.5) nm (excitation) and 510 (±5) nm (emission). Controls for monitoring DAG were made for each dilution of intact peroxisomes P5 and P6 and of the P5- and P6-based RPA and RPB, all of which contained DAG (Fig. 1 A and Fig. S3 A). The controls included the corresponding dilutions of intact peroxisomes P4 and of the P4-based RPA and RPB, all of which did not contain DAG (Fig. 1 A). Background fluorescence, which was due to the nonspecific binding of Alexa Fluor 488–tagged C1b domain to the peroxisomal membrane, was subtracted. For samples that were exposed to anti-PS mouse IgM, the pellets were resuspended in 200 μl of ice-cold buffer H and supplemented with fluorescein-conjugated goat anti–mouse IgM antibodies at 5 μg/ml. After incubation for 30 min on ice, samples were subjected to centrifugation at 100,000 *g* for 10 min at 4°C in a TLA110 rotor. The pellets were resuspended in 200 μl of ice-cold buffer H and supplemented with Alexa Fluor 488 rabbit anti-fluorescein/Oregon green IgG at 15 μg/ml. After incubation for 30 min on ice, samples were subjected to centrifugation at 100,000 *g* for 10 min at 4°C in a TLA110 rotor. The pellets were resuspended in 200 μl of ice-cold buffer H and supplemented with Alexa Fluor 488 goat anti–rabbit IgG at 20 μg/ml. After incubation for 30 min on ice, samples were subjected to centrifugation at 100,000 *g* for 10 min at 4°C in a TLA110 rotor. The pellets were resuspended in 200 μl of ice-cold buffer H and placed into the wells of a 96-well microplate. The fluorescence of samples was measured using the Victor 2 multilabel microplate fluorescence reader with filters set at 485 (±7.5) nm (excitation) and 510 (±5) nm (emission). Controls were made for each dilution of RPA, RPB, and intact peroxisomes. The controls included normal mouse IgM at 1 μg/ml added instead of anti-PS mouse IgM. Background fluorescence, which was due to the nonspecific binding of mouse IgM and/or fluorescein- or Alexa Fluor 488–labeled antibodies to the peroxisomal membrane, was subtracted.

The fraction of a monitored lipid, either DAG or PS, residing in the cytosolic leaflet of the membrane bilayer of the intact peroxisome can be calculated as follows:

$$F_{IP} \div (F_{IP} + F_{IL}), \tag{1}$$

where $F_{IP}$ is the fluorescence of a lipid-specific fluorescent probe specifically bound to intact peroxisomes or to the species of RPA and RPB that are present in the outside-out orientation. In equation 1, $F_{IP}$ equals the fluorescence of this probe specifically bound to the outer (cytosolic) leaflet of the peroxisomal membrane bilayer delimiting intact peroxisomes or those species of RPA and RPB that were resealed in the outside-out orientation. Furthermore, $F_{IL}$ in equation 1 is the fluorescence of a lipid-specific fluorescent reporter molecule that would, if it could, bind specifically to the inner (lumenal) leaflet of the peroxisomal membrane bilayer delimiting intact peroxisomes. $F_{IL}$ can be monitored by measuring the fluorescence of this reporter molecule bound to the surface of those species of RPA and RPB that were resealed in the inside-out orientation.

The value of $F_{RPA}$, the fluorescence of a lipid-specific fluorescent reporter molecule specifically bound to the surface of RPA, can be calculated as follows:

$$F_{RPA} = \left(n^{oo}{}_{RPA} \times F_{IP}\right) + \left(n^{io}{}_{RPA} \times F_{IL}\right), \tag{2}$$

where $n^{oo}{}_{RPA}$ is the fraction of the RPA species that are present in the outside-out orientation. The value of $n^{oo}{}_{RPA}$ for each of the outside-out–oriented species of RPA formed during resealing of osmotically lysed peroxisomal subforms P1–P6 was calculated for a Pex19p-specific fluorescent reporter molecule as described. The values of $n^{oo}{}_{RPA}$ for individual species of the P1- to P6-based RPA are presented in Fig. S3 (E and F). In equation 2, the value of $n^{io}{}_{RPA}$ for each of the inside-out–oriented species of RPA formed during resealing of osmotically lysed peroxisomal subforms P1–P6 was calculated for a Pex19p-specific fluorescent reporter molecule as described. The values of $n^{io}{}_{RPA}$ for individual species of P1- to P6-based RPA are presented in Fig. S3 (E and F). Based on equation 2, $F_{IL}$ can be calculated as follows:

$$F_{IL} = \frac{F_{RPA} - \left(n^{oo}{}_{RPA} \times F_{IP}\right)}{n^{io}{}_{RPA}}. \tag{3}$$

The value of $F_{RPB}$, the fluorescence of a lipid-specific fluorescent reporter molecule specifically bound to the surface of RPB, can be calculated as follows:

$$F_{RPB} = \left(n^{oo}{}_{RPB} \times F_{IP}\right) + \left(n^{io}{}_{RPB} \times F_{IL}\right), \tag{4}$$

where $n^{oo}_{RPB}$ is the fraction of the RPB species that are present in the outside-out orientation. The value of $n^{oo}_{RPB}$ for each of the outside-out–oriented species of RPB formed during resealing of osmotically lysed peroxisomal subforms P1–P6 was calculated for a Pex19p-specific fluorescent reporter molecule as described. The values of $n^{oo}_{RPB}$ for individual species of the P1- to P6-based RPA are presented in Fig. S3 (E and F). In equation 4, the value of $n^{io}_{RPB}$ for each of the inside-out–oriented species of RPB formed during resealing of osmotically lysed peroxisomal subforms P1–P6 was calculated for a Pex19p-specific fluorescent reporter molecule as described. The values of $n^{io}_{RPB}$ for individual species of P1- to P6-based RPB are presented in Fig. S3 (E and F). Based on equation 4, $F_{IL}$ can be calculated as follows:

$$F_{IL} = \frac{F_{RPB} - \left(n^{oo}{}_{RPB} \times F_{IP}\right)}{n^{io}{}_{RPB}}. \quad (5)$$

Based on equation 3, equation 1 for calculating the fraction of a monitored lipid, either DAG or PS, residing in the cytosolic leaflet of the membrane bilayer of the intact peroxisome can be rewritten as follows:

$$\frac{F_{IP}}{F_{IP} + \dfrac{F_{RPA} - \left(n^{oo}{}_{RPA} \times F_{IP}\right)}{n^{io}{}_{RPA}}}. \quad (6)$$

Furthermore, based on equation 5, equation 1 for calculating the fraction of a monitored lipid, either DAG or PS, residing in the cytosolic leaflet of the membrane bilayer of the intact peroxisome can be also rewritten as follows:

$$\frac{F_{IP}}{F_{IP} + \dfrac{F_{RPB} - \left(n^{oo}{}_{RPB} \times F_{IP}\right)}{n^{io}{}_{RPB}}}. \quad (7)$$

For each of the intact peroxisomal subforms P1–P6, equations 6 and 7 were used for calculating the fraction of a monitored lipid, either DAG or PS, residing in the cytosolic leaflet of the membrane bilayer.

**Protein-lipid overlay assay**

To evaluate the lipid-binding specificity of Pex16p, the pellet of membranes recovered after centrifugation of osmotically lysed peroxisomes was resuspended in buffer TBSO (10 mM Tris-HCl, pH 8.0, 150 mM NaCl, and 0.5% n-OG) and incubated for 30 min on ice. Samples were subjected to centrifugation at 100,000 *g* for 30 min at 4°C in a TLA110 rotor. Under these conditions, n-OG completely solubilized the vast majority of all membrane proteins (Boukh-Viner et al., 2005). The supernatants of n-OG–solubilized proteins were then incubated at 5 μg/ml with the PIP Strips at 4°C overnight. After washing the PIP Strip five times for 5 min each with TBSO, Pex16p was detected by immunoblotting with anti-Pex16p antibodies.

**Purification of LPAAT and PAP**

For purification of LPAAT, highly purified mature peroxisomes P6 were lysed by the addition of 10 vol of ice-cold LB buffer, followed by incubation on ice for 30 min with occasional agitation. The suspension was centrifuged at 200,000 *g* for 20 min at 4°C in a TLA110 rotor. The pellet of membranes recovered after centrifugation of osmotically lysed peroxisomes was resuspended in ice-cold HAT + C buffer (20 mM Hepes-KOH, pH 7.4, 2 mM EDTA, 1 mM DTT, 10% [wt/vol] glycerol, and 0.5% [wt/vol] $Na^+$ cholate) to a final concentration of 5.0 mg/ml. After incubation on ice for 30 min with occasional agitation, the sample was subjected to centrifugation at 100,000 *g* for 30 min at 4°C in a TLA110 rotor. The recovered supernatant of detergent-solubilized PMPs was applied to a Resource S column, which was preequilibrated with 10 column volumes of HAT − C buffer (20 mM Hepes-KOH, pH 7.4, 2 mM EDTA, 1 mM DTT, and 10% [wt/vol] glycerol) followed by 1 column volume of HAT + C buffer. The column was washed with 4 column volumes of HAT + C buffer followed by elution of LPAAT activity with a linear 0–1 M NaCl gradient in HAT + C buffer. The peak of LPAAT activity eluted from the column in a NaCl concentration of 225 mM. LPAAT-containing fractions were combined, dialyzed against HPC + C buffer (20 mM Hepes-KOH, pH 7.4, 50 mM KCl, 25 mM KOAc, 3 mM $MgCl_2$, 2 mM MgOAc, 1 mM DTT, 10% [wt/vol] glycerol, and 0.5% [wt/vol] $Na^+$ cholate), and applied to a palmitoyl-CoA agarose column, which was preequilibrated with 5 column volumes of HPC − C buffer (20 mM Hepes-KOH, pH 7.4, 50 mM KCl, 25 mM KOAc, 3 mM $MgCl_2$, 2 mM MgOAc, 1 mM DTT, and 10% [wt/vol] glycerol) followed by 1 column volume of HPC + C buffer. The column was washed with 9 column volumes of HPC + C buffer followed by 1 column volume of HPC + C buffer containing 0.5 mM free palmitoyl-CoA. The column was kept for 6 h at 4°C. LPAAT activity was eluted with 2 column volumes of HPC + C buffer containing 5 mM free palmitoyl-CoA followed by 2 column volumes of HPC + C buffer alone. The two LPAAT-containing eluates were pooled and stored at −80°C, before being analyzed by SDS-PAGE followed by silver staining and mass spectrometric identification of LPAAT. A summary of the purification of LPAAT is presented in Fig. 2 A. The overall purification of LPAAT over the $Na^+$-extracted membrane of mature peroxisomes P6 was 232-fold.

For purification of PAP, highly purified mature peroxisomes P6 were lysed by the addition of 10 vol of ice-cold LB buffer, followed by incubation on ice for 30 min with occasional agitation. The suspension was centrifuged at 200,000 *g* for 20 min at 4°C in a TLA110 rotor. The pellet of membranes recovered after centrifugation of osmotically lysed peroxisomes was resuspended in ice-cold TP + C buffer (20 mM Tris-HCl, pH 7.4, 3 mM $MgCl_2$, 2 mM MgOAc, 1 mM DTT, 10% [wt/vol] glycerol, and 0.5% [wt/vol] $Na^+$ cholate) to a final concentration of 5.0 mg/ml. After incubation on ice for 30 min with occasional agitation, the sample was subjected to centrifugation at 100,000 *g* for 30 min at 4°C in a TLA110 rotor. The recovered supernatant of detergent-solubilized PMPs was applied to a Resource Q column, which was preequilibrated with 5 column volumes of TP − C buffer (20 mM Tris-HCl, pH 7.4, 3 mM $MgCl_2$, 2 mM MgOAc, 1 mM DTT, and 10% [wt/vol] glycerol) followed by 1 column volume of TP + C buffer. The column was washed with 5 column volumes of TP + C buffer followed by elution of PAP activity with a linear 0–0.5 M NaCl gradient in TP + C buffer. The peak of PAP activity eluted from the column in a NaCl concentration of 110 mM. PAP-containing fractions were combined, dialyzed against PPS + C buffer (10 mM potassium phosphate, pH 7.0, 100 mM KCl, 3 mM $MgCl_2$, 2 mM MgOAc, 1 mM DTT, 10% [wt/vol] glycerol, and 0.5% [wt/vol] $Na^+$ cholate), and applied to a HiTrap Blue HP column, which was preequilibrated with 5 column volumes of PPS − C buffer (10 mM potassium phosphate, pH 7.0, 100 mM KCl, 3 mM $MgCl_2$, 2 mM MgOAc, 1 mM DTT, and 10% [wt/vol] glycerol) followed by 1 column volume of PPS + C buffer. The column was washed with 5 column volumes of PPS + C buffer followed by elution of PAP activity with a linear 0.1–1.5 M KCl gradient in PPS + C buffer. The peak of PAP activity eluted from the column in a KCl concentration of 660 mM. PAP-containing fractions were pooled, dialyzed against PP + C buffer (10 mM potassium phosphate, pH 7.0, 5 mM $MgCl_2$, 5 mM MgOAc, 1 mM DTT, 10% [wt/vol] glycerol, and 0.5% [wt/vol] $Na^+$ cholate), and applied to a hydroxylapatite column, which was preequilibrated with 5 column volumes of PP + C buffer. The column was washed with 3 column volumes of PP + C buffer followed by elution of PAP activity with 10 column volumes of a linear 10–200 mM potassium phosphate gradient in PP + C buffer. The peak of PAP activity eluted from the column in a potassium phosphate concentration of 95 mM. PAP-containing fractions were combined, dialyzed against TPM + C buffer (25 mM Tris-HCl, pH 7.4, 10 mM $MgCl_2$, 10 mM MgOAc, 1 mM DTT, 10% [wt/vol] glycerol, and 0.5% [wt/vol] $Na^+$ cholate), and applied to a Superose 12 column, which was preequilibrated with 5 column volumes of TPM + C buffer. PAP was eluted from the column with TPM + C buffer. PAP-containing fractions were pooled and stored at −80°C before being analyzed by SDS-PAGE followed by silver staining and mass spectrometric identification of PAP. A summary of the purification of PAP is presented in Fig. 2 A. The overall purification of PAP over the $Na^+$-extracted membrane of mature peroxisomes P6 was 423-fold.

**Chemical cross-linking and immunoprecipitation under denaturing conditions**

For identifying components of the peroxisomal membrane that interact with Vps1p, Pex10p, or Pex19p, highly purified mature peroxisomes of wild-type and mutant strains were osmotically lysed by the addition of 10 vol of ice-cold LCC buffer (20 mM sodium phosphate buffer, pH 7.5, and 150 mM NaCl), followed by incubation on ice for 30 min with occasional agitation. The suspension was centrifuged at 200,000 *g* for 20 min at 4°C in a TLA110 rotor. The pellet of membranes recovered after centrifugation of osmotically lysed peroxisomes was resuspended in ice-cold LCC buffer to a final concentration of 0.5 mg/ml. For identifying proteins that interact with Vps1p or Pex19p in the cytosol, wild- type and mutant cells were subjected to subcellular fractionation (see Subcellular fractionation...) to yield the 200S (cytosolic) fraction in buffer H containing 1 M sorbitol. 9 vol of ice-cold LCC buffer was added to the recovered cytosolic fraction.

Cross-linking of membrane-associated or cytosolic proteins with the thiol-cleavable cross-linker DSP (Pierce Chemical Co.) was initiated by the addition of cross-linker (50 mM stock in DMSO) and continued for 1 h at 4°C. Cross-linking was quenched by the addition of 0.1 vol of 1 M Tris-HCl, pH 7.5, and incubation for 30 min at 4°C. SDS was added to 1.25%, and samples were warmed at 65°C for 20 min and then cooled to room temperature. 4 vol of 60 mM Tris-HCl, pH 7.4, 1.25% (vol/vol) Triton X-100, 190 mM NaCl, and 6 mM EDTA was added to the cooled samples, which were then cleared of any nonspecifically binding proteins by incubation for 20 min at 4° C with protein A–Sepharose washed five times with 10 mM Tris-HCl, pH 7.5. The cleared samples were then subjected to immunoprecipitation with anti-Vps1p, anti-Pex10p, or anti-Pex19p antibodies under denaturing, nonreducing conditions. These antibodies were covalently linked to protein A–Sepharose as described previously (Xu et al., 1998). Bound proteins were washed five times with 50 mM Tris-HCl, pH 7.5, 150 mM NaCl, and 1% (vol/vol) Triton X-100 and eluted with 2% SDS at 95°C for 5 min. Eluted proteins were analyzed by SDS- PAGE under reducing conditions, i.e., with DTT in the sample buffer, followed by silver staining.

**Mass spectrometry**

Proteins were resolved by SDS-PAGE and visualized by silver staining (Shevchenko et al., 1996). Protein bands were excised from the gel, reduced, alkylated, and in gel–digested with trypsin (Shevchenko et al., 1996). The proteins were identified by matrix-assisted laser desorption/ionization mass spectrometric peptide mapping (Jiménez et al., 1998), using a Micromass M@LDI time-of-flight mass spectrometer (Waters). Database searching using peptide masses was performed with the Mascot web-based search engine.

The identification of Sla1p by mass spectrometric peptide mapping was based on the analysis of 14 peptides of a 138-kD protein. These peptides covered 19% of the Sla1p sequence with mass accuracy better than 100 ppm over the mass to charge ratio range of 1,000 to 2,400. 11 peptides of a 81-kD protein that were used for the identification of Vps1p covered 23% of the protein sequence with mass accuracy better than 100 ppm over the mass to charge ratio range of 700 to 2,200. Nine peptides of a 53-kD protein that were used for the identification of Abp1p covered 27% of the protein sequence with mass accuracy better than 100 ppm over the mass to charge ratio range of 800 to 2,100. 10 peptides of a 47-kD protein that were used for the identification of Pex19p covered 32% of the protein sequence with mass accuracy better than 100 ppm over the mass to charge ratio range of 900 to 2,300. Eight peptides of a 41-kD protein that were used for the identification of Act1p covered 29% of the protein sequence with mass accuracy better than 100 ppm over the mass to charge ratio range of 1,000 to 2,100. 10 peptides of a 40-kD protein that were used for the identification of Slc1p (LPAAT) covered 42% of the protein sequence with mass accuracy better than 100 ppm over the mass to charge ratio range of 800 to 2,200. 10 peptides of a 37-kD protein that were used for the identification of Pex10p covered 38% of the protein sequence with mass accuracy better than 100 ppm over the mass to charge ratio range of 800 to 2,300. Seven peptides of a 33-kD protein that were used for the identification of Dpp1p (PAP) covered 32% of the protein sequence with mass accuracy better than 100 ppm over the mass to charge ratio range of 600 to 2,600.

**Electron microscopy and morphometric analysis**

Whole cells were fixed in 1.5% $KMnO_4$ for 20 min at room temperature, dehydrated by successive incubations in increasing concentrations of ethanol, and embedded in Poly/Bed 812 epoxy resin (Polysciences). Ultrathin sections were cut using an Ultra-Cut E Microtome (Reichert-Jung). Silver/gold thin sections from the embedded blocks were examined in a transmission electron microscope (JEM-2000FX; JEOL).

For morphometric analysis of random electron microscopic sections of cells, 12- × 14-cm prints and 8- × 10-cm negatives of 35–40 cell sections of each strain at 24,000–29,000 magnification were scanned and converted to digitized images with a ScanJet 4400c (Hewlett-Packard) and Photoshop 6.0 software (Adobe Systems, Inc.). Quantitation of digitized images was performed using the Discovery Series Quantity One 1-D Analysis Software (Bio-Rad Laboratories). Relative area of peroxisome section (as a percentage) was calculated as the area of peroxisome section/area of cell section × 100. Peroxisomes were counted in electron micrographs, and data are expressed as the number of peroxisomes per $\mu m^3$ of cell section volume.

Resealed peroxisomes RPA and RPB floated to low density during centrifugation in a multistep sucrose density gradient. A 200-μl aliquot of the peak fraction of purified RPA in MR buffer or a 200-μl aliquot of the peak fraction of purified RPB in HR buffer was mixed with 400 μl of ice-cold 150 mM sodium cacodylate buffer, pH 7.2, containing 3% glutaraldehyde. Immediately after mixing the sample and glutaraldehyde solution, 600 μl of 2% $OsO_4$ in ice-cold CD buffer (100 mM sodium cacodylate, pH 7.2) was added. After a 2-h incubation on ice, the resealed peroxisomes RPA and RPB were sedimented at 100,000 *g* for 20 min at 4°C in a TLS55 rotor (Beckman Coulter) onto a bed (25–50 μl) of hardened, low-melting 2.5% NuSieve GTG agarose (FMC). The pellet was postfixed in a solution of 1% $OsO_4$ plus 2.5% $K_2Cr_2O_7$ in ice-cold CD buffer for 2 h on ice. The pellet was then rinsed twice with ice-cold CD buffer and exposed to 0.05% tannic acid in the same buffer. After a 30-min incubation on ice, the pellet was washed once with ice-cold CD buffer and three times with water. The pellet was incubated overnight with 2% uranyl acetate in water at 4°C and then washed three times with water. After dehydration in a graded ethanol series, the fixed and stained sample was embedded in Poly/Bed 812 epoxy resin (Polysciences). Silver/gold thin sections from the embedded blocks were examined in the JEM-2000FX transmission electron microscope.

**Online supplemental material**

Fig. S1 shows that the peroxisomal membrane lacks the activities of enzymes that, in addition to LPAAT and PAP, can catalyze reactions resulting in the formation of PA or DAG. Fig. S2 demonstrates the effect of the *slc1Δ*, *dpp1Δ*, *vps1Δ*, *sla1Δ*, and *abp1Δ* mutations on the size and number of peroxisomes. Fig. S3 documents the dynamics of changes in the transbilayer distribution of DAG and PS in the peroxisomal membrane during peroxisome maturation. Fig. S4 provides evidence that the Pex2p-dependent transfer of PC from a P3- and P4-associated subcompartment of the ER provides the peroxisomal membrane with the bulk quantities of this lipid. Fig. S5 shows that only division-competent mature peroxisomes recruit Vps1p from the cytosol to the outer face of their membrane. Online supplemental material is available at http://www.jcb.org/cgi/content/full/jcb.200609072/DC1.

We are grateful to Dr. Alexandra C. Newton for the GST-C1B vector, Dr. Jean-Marc Nicaud for the *pex10Δ* and *vps1Δ* mutant strains, and Dr. Richard A. Rachubinski for antibodies to Pex2p, Pex16p, Pex19p, and thiolase.

This work was supported by grants from the Canadian Institutes of Health Research (MOP-57662) and the Natural Sciences and Engineering Research Council of Canada (NSERC 283228) to V.I. Titorenko.

Submitted: 12 September 2006
Accepted: 19 March 2007

## References

Athenstaedt, K., and G. Daum. 1999. Phosphatidic acid, a key intermediate in lipid metabolism. *Eur. J. Biochem.* 266:1–16.

Bankaitis, V.A. 2002. Slick recruitment to the Golgi. *Science.* 295:290–291.

Behnia, R., and S. Munro. 2005. Organelle identity and the signposts for membrane traffic. *Nature.* 438:597–604.

Boukh-Viner, T., T. Guo, A. Alexandrian, A. Cerracchio, C. Gregg, S. Haile, R. Kyskan, S. Milijevic, D. Oren, J. Solomon, et al. 2005. Dynamic ergosterol- and ceramide-rich domains in the peroxisomal membrane serve as an organizing platform for peroxisome fusion. *J. Cell Biol.* 168:761–773.

Carman, G.M., and G.S. Han. 2006. Roles of phosphatidate phosphatase enzymes in lipid metabolism. *Trends Biochem. Sci.* 31:694–699.

Chernomordik, L.V., and M.M. Kozlov. 2003. Protein-lipid interplay in fusion and fission of biological membranes. *Annu. Rev. Biochem.* 72:175–207.

Colanzi, A., C. Suetterlin, and V. Malhotra. 2003. Cell-cycle-specific Golgi fragmentation: how and why? *Curr. Opin. Cell Biol.* 15:462–467.

Corda, D., A. Colanzi, and A. Luini. 2006. The multiple activities of CtBP/BARS proteins: the Golgi view. *Trends Cell Biol.* 16:167–173.

De Matteis, M., A. Godi, and D. Corda. 2002. Phosphoinositides and the Golgi complex. *Curr. Opin. Cell Biol.* 14:434–447.

Diaz Anel, A.M., and V. Malhotra. 2005. PKCη is required for β1γ2/β3γ2- and PKD-mediated transport to the cell surface and the organization of the Golgi apparatus. *J. Cell Biol.* 169:83–91.

Eitzen, G.A., R.K. Szilard, and R.A. Rachubinski. 1997. Enlarged peroxisomes are present in oleic acid-grown *Yarrowia lipolytica* overexpressing the *PEX16* gene encoding an intraperoxisomal peripheral membrane peroxin. *J. Cell Biol.* 137:1265–1278.

Farsad, K., and P. De Camilli. 2003. Mechanisms of membrane deformation. *Curr. Opin. Cell Biol.* 15:372–381.

Fratti, R.A., Y. Jun, A.J. Merz, N. Margolis, and W. Wickner. 2004. Interdependent assembly of specific regulatory lipids and membrane fusion proteins into the vertex ring domain of docked vacuoles. *J. Cell Biol.* 167:1087–1098.

Fried, B., and J. Sherma. 1999. Thin-Layer Chromatography. Marcel Dekker, Inc., New York. 499 pp.

Guo, T., Y.Y. Kit, J.-M. Nicaud, M.-T. Le Dall, S.K. Sears, H. Vali, H. Chan, R.A. Rachubinski, and V.I. Titorenko. 2003. Peroxisome division in the yeast *Yarrowia lipolytica* is regulated by a signal from inside the peroxisome. *J. Cell Biol.* 162:1255–1266.

Hannun, Y.A., C. Luberto, and K.M. Argraves. 2001. Enzymes of sphingolipid metabolism: from modular to integrative signaling. *Biochemistry.* 40:4893–4903.

Hoepfner, D., M. van den Berg, P. Philippsen, H.F. Tabak, and E.H. Hettema. 2001. A role for Vps1p, actin, and the Myo2p motor in peroxisome abundance and inheritance in *Saccharomyces cerevisiae*. *J. Cell Biol.* 155:979–990.

Holthuis, J.C., and T.P. Levine. 2005. Lipid traffic: floppy drives and a superhighway. *Nat. Rev. Mol. Cell Biol.* 6:209–220.

Jiménez, C.R., L. Huang, Y. Qiu, and A.L. Burlingame. 1998. Searching sequence databases over the Internet: protein identification using MS-Fit. *In* Current Protocols in Protein Science. J.E. Coligan, B.M. Dunn, H.L. Ploegh, D.W. Speicher, and P.T. Wigfield, editors. John Wiley and Sons, New York. 16.5.1–16.5.6.

Johnson, J.E., J. Giorgione, and A.C. Newton. 2000. The C1 and C2 domains of protein kinase C are independent membrane targeting modules, with specificity for phosphatidylserine conferred by the C1 domain. *Biochemistry.* 39:11360–11369.

Kooijman, E.E., V. Chupin, B. de Kruijff, and K.N.J. Burger. 2003. Modulation of membrane curvature by phosphatidic acid and lysophosphatidic acid. *Traffic.* 4:162–174.

Lambkin, G.R., and R.A. Rachubinski. 2001. *Yarrowia lipolytica* cells mutant for the peroxisomal peroxin Pex19p contain structures resembling wild-type peroxisomes. *Mol. Biol. Cell.* 12:3353–3364.

McMahon, H.T., and J.L. Gallop. 2005. Membrane curvature and mechanisms of dynamic cell membrane remodelling. *Nature.* 438:590–596.

Munro, S. 2003. Earthworms and lipid couriers. *Nature.* 426:775–776.

Newmyer, S.L., A. Christensen, and S. Sever. 2003. Auxilin-dynamin interactions link the uncoating ATPase chaperone machinery with vesicle formation. *Dev. Cell.* 4:929–940.

Olazabal, I.M., and L.M. Machesky. 2001. Abp1p and cortactin, new "handholds" for actin. *J. Cell Biol.* 154:679–682.

Osteryoung, K.W., and J. Nunnari. 2003. The division of endosymbiotic organelles. *Science.* 302:1698–1704.

Peters, C., T.L. Baars, S. Bühler, and A. Mayer. 2004. Mutual control of membrane fission and fusion proteins. *Cell.* 119:667–678.

Praefcke, G.J., and H.T. McMahon. 2004. The dynamin superfamily: universal membrane tubulation and fission molecules? *Nat. Rev. Mol. Cell Biol.* 5:133–147.

Pruyne, D., and A. Bretscher. 2000. Polarization of cell growth in yeast. I. Establishment and maintenance of polarity states. *J. Cell Sci.* 113:365–375.

Rieder, S.E., and S.D. Emr. 2000. Isolation of subcellular fractions from the yeast *Saccharomyces cerevisiae*. *In* Current Protocols in Cell Biology. J.S. Bonifacino, M. Dasso, J.B. Harford, J. Lippincott-Schwartz, and K.M. Yamada, editors. John Wiley and Sons, New York. 3.8.1–3.8.68.

Schneiter, R., B. Brugger, R. Sandhoff, G. Zellnig, A. Leber, M. Lampl, K. Athenstaedt, C. Hrastnik, S. Eder, G. Daum, et al. 1999. Electrospray ionization tandem mass spectrometry (ESI-MS/MS) analysis of the lipid molecular species composition of yeast subcellular membranes reveals acyl chain-based sorting/remodeling of distinct molecular species en route to the plasma membrane. *J. Cell Biol.* 146:741–754.

Schrader, M. 2006. Shared components of mitochondrial and peroxisomal division. *Biochim. Biophys. Acta.* 1763:531–541.

Shemesh, T., A. Luini, V. Malhotra, K.N. Burger, and M.M. Kozlov. 2003. Prefission constriction of Golgi tubular carriers driven by local lipid metabolism: a theoretical model. *Biophys. J.* 85:3813–3827.

Shevchenko, A., O.N. Jensen, A.V. Podtelejnikov, F. Sagliocco, M. Wilm, O. Vorm, P. Mortensen, A. Shevchenko, H. Boucherie, and M. Mann. 1996. Linking genome and proteome by mass spectrometry: large-scale identification of yeast proteins from two dimensional gels. *Proc. Natl. Acad. Sci. USA.* 93:14440–14445.

Shorter, J., and G. Warren. 2002. Golgi architecture and inheritance. *Annu. Rev. Cell Dev. Biol.* 18:379–420.

Sillence, D.J., and F.M. Platt. 2004. Glycosphingolipids in endocytic membrane transport. *Semin. Cell Dev. Biol.* 15:409–416.

Sprong, H., P. van der Sluijs, and G. van Meer. 2001. How proteins move lipids and lipids move proteins. *Nat. Rev. Mol. Cell Biol.* 2:504–513.

Subramani, S., A. Koller, and W.B. Snyder. 2000. Import of peroxisomal matrix and membrane proteins. *Annu. Rev. Biochem.* 69:399–418.

Szilard, R.K., V.I. Titorenko, M. Veenhuis, and R.A. Rachubinski. 1995. Pay32p of the yeast *Yarrowia lipolytica* is an intraperoxisomal component of the matrix protein translocation machinery. *J. Cell Biol.* 131:1453–1469.

Thoms, S., and R. Erdmann. 2005. Dynamin-related proteins and Pex11 proteins in peroxisome division and proliferation. *FEBS J.* 272:5169–5181.

Titorenko, V.I., and R.T. Mullen. 2006. Peroxisome biogenesis: the peroxisomal endomembrane system and the role of the ER. *J. Cell Biol.* 174:11–17.

Titorenko, V.I., G.A. Eitzen, and R.A. Rachubinski. 1996. Mutations in the *PAY5* gene of the yeast *Yarrowia lipolytica* cause the accumulation of multiple subpopulations of peroxisomes. *J. Biol. Chem.* 271:20307–20314.

Titorenko, V.I., J.J. Smith, R.K. Szilard, and R.A. Rachubinski. 1998. Pex20p of the yeast *Yarrowia lipolytica* is required for the oligomerization of thiolase in the cytosol and for its targeting to the peroxisome. *J. Cell Biol.* 142:403–420.

Titorenko, V.I., H. Chan, and R.A. Rachubinski. 2000. Fusion of small peroxisomal vesicles in vitro reconstructs an early step in the in vivo multistep peroxisome assembly pathway of *Yarrowia lipolytica*. *J. Cell Biol.* 148:29–43.

van Meer, G., and H. Sprong. 2004. Membrane lipids and vesicular traffic. *Curr. Opin. Cell Biol.* 16:373–378.

Voelker, D.R. 2005. Bridging gaps in phospholipid transport. *Trends Biochem. Sci.* 30:396–404.

Wang, H.J., M.-T. Le Dall, Y. Waché, C. Laroche, J.-M. Belin, C. Gaillardin, and J.-M. Nicaud. 1999. Evaluation of acyl coenzyme A oxidase (Aox) isozyme function in the *n*-alkane-assimilating yeast *Yarrowia lipolytica*. *J. Bacteriol.* 181:5140–5148.

Warren, D.T., P.D. Andrews, C.W. Gourlay, and K.R. Ayscough. 2002. Sla1p couples the yeast endocytic machinery to proteins regulating actin dynamics. *J. Cell Sci.* 115:1703–1715.

Xu, Z., K. Sato, and W. Wickner. 1998. LMA1 binds to vacuoles at Sec18p (NSF), transfers upon ATP hydrolysis to a t-SNARE (Vam3p) complex, and is released during fusion. *Cell.* 93:1125–1134.

Yan, M., N. Rayapuram, and S. Subramani. 2005. The control of peroxisome number and size during division and proliferation. *Curr. Opin. Cell Biol.* 17:376–383.

Youle, R.J., and M. Karbowski. 2005. Mitochondrial fission in apoptosis. *Nat. Rev. Mol. Cell Biol.* 6:657–663.

Zimmerberg, J., and M.M. Kozlov. 2006. How proteins produce cellular membrane curvature. *Nat. Rev. Mol. Cell Biol.* 7:9–19.